REPORT SNO 6758-2014

Bottom RedOx Model (BROM) general description and application for seasonal anoxia simulations

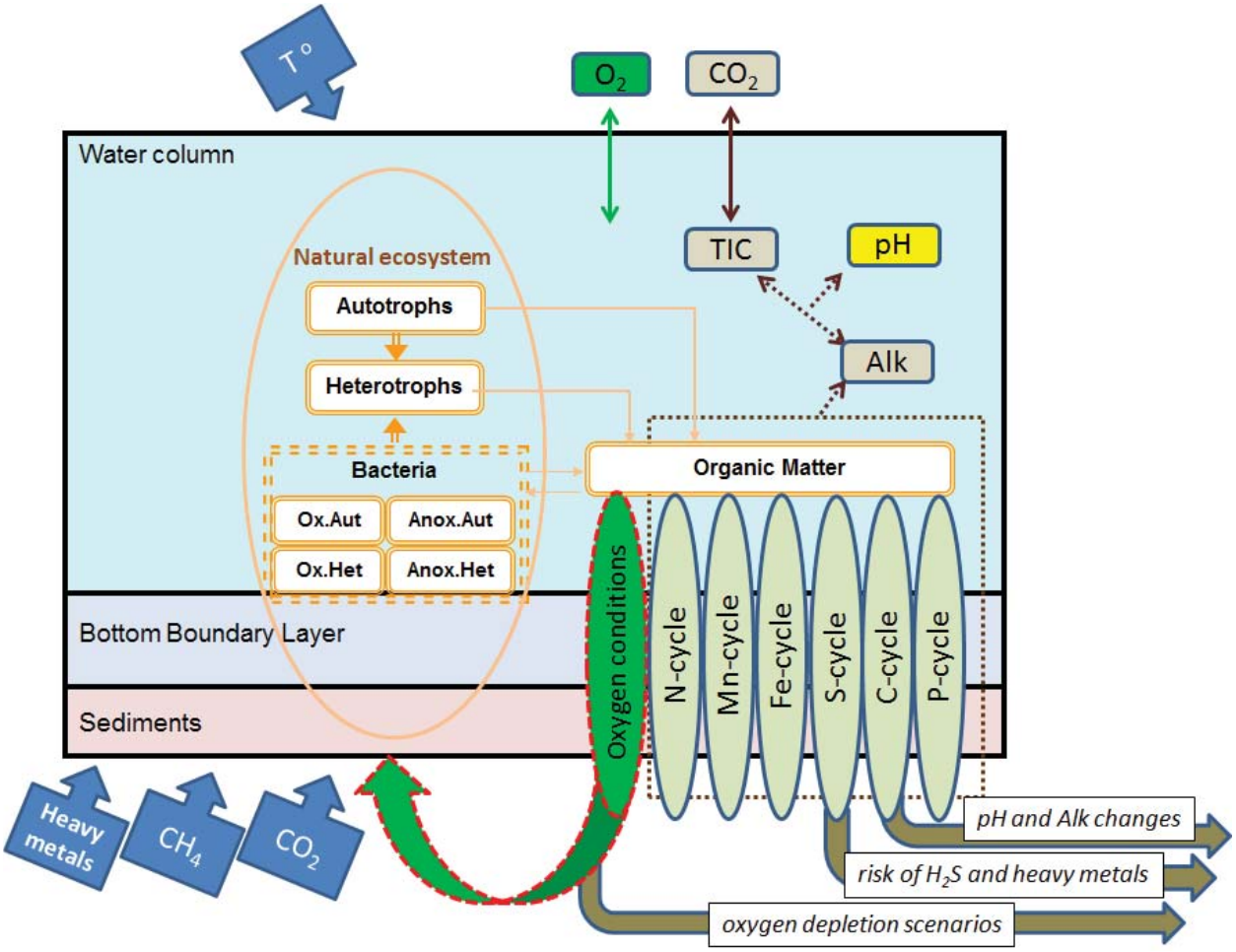

Norwegian Institute for Water Research
– an institute in the Environmental Research Alliance of Norway

REPORT

Main Office
Gaustadalléen 21
NO-0349 Oslo, Norway
Phone (47) 22 18 51 00
Telefax (47) 22 18 52 00
Internet: www.niva.no

NIVA Region South
Jon Lilletuns vei 3
NO-4879 Grimstad, Norway
Phone (47) 22 18 51 00
Telefax (47) 37 04 45 13

NIVA Region East
Sandvikaveien 59
NO-2312 Ottestad, Norway
Phone (47) 22 18 51 00
Telefax (47) 62 57 66 53

NIVA Region West
Thormøhlens gate 53 D
NO-5006 Bergen Norway
Phone (47) 22 18 51 00
Telefax (47) 55 31 22 14

Title	Report No..	Date
Bottom RedOx Model (BROM) general description and application for seasonal anoxia simulations	6758-2014	08.12.2014
	Project No. 29133, 11121, 14020, 14371	Pages Price 46
Author(s) E.V.Yakushev* , E.A. Protsenko**, J. Bruggeman*** *Norwegian Institute for water Research (NIVA) **Shirshov Institute of Oceanology RAS (SIO RAS) ***Plymouth Marine Laboratory (PML)	Topic group Oceanography, biogeochemistry	Distribution Open
	Geographical area North Sea	Printed NIVA

Client(s)	Client ref.
NIVA	

Abstract
The details of biogeochemical transfer of matter at the sediment-water boundary were modelled by a one-dimensional C-N-P-Si-O-S-Mn-Fe vertical transport-reaction model for describing both the sediments and bottom boundary layers coupled with biogeochemical block simulating changeable redox conditions, and the carbonate system processes block. It was shown that seasonality in production and decay of organic matter significantly affects the redox conditions and the chemical species distributions and fluxes.

4 keywords, Norwegian	4 keywords, English
1. biogeokjemiske modellering	1. biogeochemical modelling
2. redoks prosesser	2. redox processes
3. ph og alkalitet	3. pH and alkalinity
4. næringsstoffer	4. nutrients

Evgeny Yakushev
Project Manager

Kai Sørensen
Research Manager

ISBN 978-82-577-6493-7

Bottom RedOx Model (BROM) general description and application for seasonal anoxia simulations

Preface

The goal of this work was to develop a model that captures the key biogeochemical processes occurring at the sediment-water interface and to apply it to analyse the changes that result from seasonal oscillations in redox conditions. This report presents the description of this Bottom RedOx Model, BROM, a one-dimensional coupled biogeochemical transport model, that considered cycles of several chemical elements i.e. C, N, P, O, Si, Fe, Mn, S simultaneously. BROM is being used in the Projects: FP7 'Sub-seabed CO2 Storage: Impact on Marine Ecosystems', ECO2, FP7 'Research into Impacts and Safety in CO_2 Storage', RISCS, FME SUCCESS, CO2Base, EEA CO2MARINE.

NIVA has coordinated the project, with P.P.Shirshov Institute of Oceanology of the Russian Academy of Sciences (SIO RAS) and Plymouth Marine Laboratory (PML) as partners. The project team has included

NIVA	Evgeniy Yakushev
SIO RAS	Elizaveta Protsenko
PML	Jorn Bruggeman

Thanks to the funding institutions and all project participants for their valuable contributions to the project! Thanks also to Dr. Philip Wallhead for carrying out quality assurance of the report.

Evgeny Yakushev
Oslo, 08.12.2014

Contents

Summary

Interaction between seawater and sediments plays an important role in global biogeochemical cycling. The benthic fluxes of chemical elements (C,N,P,O,Si,Fe,Mn) directly affect acidification (i.e. pH and carbonate saturation) and redox state, which in turn determine the functioning of the benthic and pelagic ecosystems. The redox state of the near bottom layer can change and oscillate in many regions in connection with supply of organic matter (OM), physical regime and coastal discharge influence. The goal of this work was to develop a model that captures the key biogeochemical processes occurring at the sediment-water interface and to apply it to analyse the changes that result from seasonal oscillations in redox conditions.

The model simulated several well-known features of the seasonality of temperate ecosystems, i.e. an increase in the concentration of phototrophic organisms in summer, production of excessive OM and summer development of heterotrophic organisms and heterotrophic bacteria. These changes were driven by physical conditions, with the hydrodynamic model reproducing intensive vertical mixing in winter and formation of a pycnocline in summer. Through model simulations it was shown that the seasonality in production and destruction of OM together with the mixing seasonality leads to variation of redox conditions in the bottom boundary layer (BBL). Bacteria play a significant role in the fate of OM due to chemosynthesis (autotrophs) and consumption of DOM (heterotrophs).

Changes in the bottom boundary layer redox conditions affect distribution of nutrients (N and P), redox metals (Mn and Fe). Model can be used for analysing and interpreting data on sediment-water exchange and estimating consequences of forcing (i.e. climate change, ocean acidification, CCS leakages, local pollution with hazardous substances).

1. Background

Oxygen depletion and anoxia are increasingly common features observed in the World Ocean, inland seas and coastal areas. Observations show a decline in the dissolved oxygen concentrations at continental margins in many regions and these are related to both an increase in anthropogenic nutrient loadings and a decrease in vertical mixing e.g., (Diaz and Rosenberg, 2008; Rabalais et al., 2002; Richardson and Jørgensen, 1996).

Although bottom waters may be permanently oxic or anoxic, near-bottom conditions oscillate seasonally between these extremes in many water bodies (Morse and Eldridge, 2007). Such oscillations typically result from variation in the supply of organic matter (OM), physical regime and river run-off. Frequently, oxic conditions during periods of intense mixing are followed by near-bottom suboxia or anoxia after the seasonal pycnocline forms, restricting aeration of the deeper layers. This occurs for instance in the Louisiana shelf (Morse and Eldridge, 2007), Corpus Christi Bay (McCarthy et al., 2008), the Sea of Azov (Debolskaya et al., 2008), and Elefsis Bay (Pavlidou et al., 2013).

The redox state and oxygenation of near-bottom water is directly affected by transport of oxidized and reduced species across the sediment–water interface and, consequently, by biogeochemical processes occurring in the sediment itself (Cooper and Morse, 1996; Jorgensen et al., 1990; Roden and Tuttle, 1992; Sell and Morse, 2006). For example, when mixing rates are low, bottom water oxygen depletion associated with local OM mineralization, combined with a high benthic oxygen demand (BOD) associated with heterotrophic oxidation of sedimentary OM, can cause anoxia in the bottom water. This leads to the death or flight of benthic macro and meio faunal organisms responsible for bioturbation and bioirrigation (Blackwelder et al., 1996; Morse and Eldridge, 2007; SenGupta et al., 1996) which can greatly slow oxidative reactions and transport of solid and dissolved species inside the sediments. Under such conditions, sedimentary sulfides can build up and dissolution of carbonate minerals may become slow or pause (Morse and Eldridge, 2007).

When oxic conditions return there can be a major "oxygen debt" of reduced species in the water column (Yakushev et al., 2011) and at the sediment–water interface that may buffer and postpone the reestablishment of the previous oxic conditions in the sediments(Morse and Eldridge, 2007). In areas with seasonal hypoxia/anoxia, the processes taking place in the water column and in the sediments are clearly interconnected. However, a quantitative understanding of the dynamics of the physical, chemical and biological processes in these environments with changing redox conditions is not well established. This is the gap we aim to address with this work.

The study of the processes responsible for changing of redox conditions from oxic to anoxic should be supplemented by modelling to allow a joint analysis of the complex processes studied by the different scientific disciplines. Of course, the models are simplifications of real system, sometimes overemphasizing particular characteristics, as in a caricature. Nevertheless, modeling seems to be appropriate for use as a diagnostic tool able to study and analyse every feature of the system, even variables and fluxes that are hard or impossible to measure. Models can be used for testing the hypothesis of which processes are responsible for the observed distributions (Yakushev and Newton, 2013) and to produce predictions of future system state, or the ability to evaluate scenarios ("what if…"). Thus, modelling and observations mutually complement each other.

A number of recent studies demonstrates the capability of sophisticated reactive transport codes for integrated modelling of biogeochemical cycles in sediments (Boudreau, 1996; Couture et al., 2010; Pena et al., 2010; Soetaert et al., 1996; Van Cappellen and Wang, 1996; Van Der Loeff and Boudreau, 1997), but nevertheless the question of an influence of changeable redox conditions remains open with an exception of a modeling study by (Katsev et al., 2007). The water column redox interface was studied in the models (Konovalov et al., 2006; Yakushev, 2006; Yakushev et al., 2007).

However, the Bottom Boundary Layer (BBL) – a thin layer of water with the steepest gradients and the greatest fluctuations in redox conditions – is still unexplored. In this work, we aim to fill this gap by developing a unified model of ecosystem dynamics and redox chemistry that considers these three layers (pelagic, BBL, sediment) together . This allows us to investigate the dynamics of the part of the water column that is critical for ecosystem functioning, yet hard-to-reach for in-situ exploration. This work aims to merge existing approaches in order to simultaneously describe the processes occurring in the water column and in the upper layer of the sediments. The main focus of this investigation relates to the BBL, the most active zone of interactions. Although the biogeochemical module of the model considers an extensive list of compounds and fluxes (**Figure 1**), we concentrate in this paper on description of the fate of the species of the most important elements responsible for the changes of the redox conditions – oxygen, nitrogen, sulfur, manganese, iron - and describe the changes in the alkalinity and carbonate system.

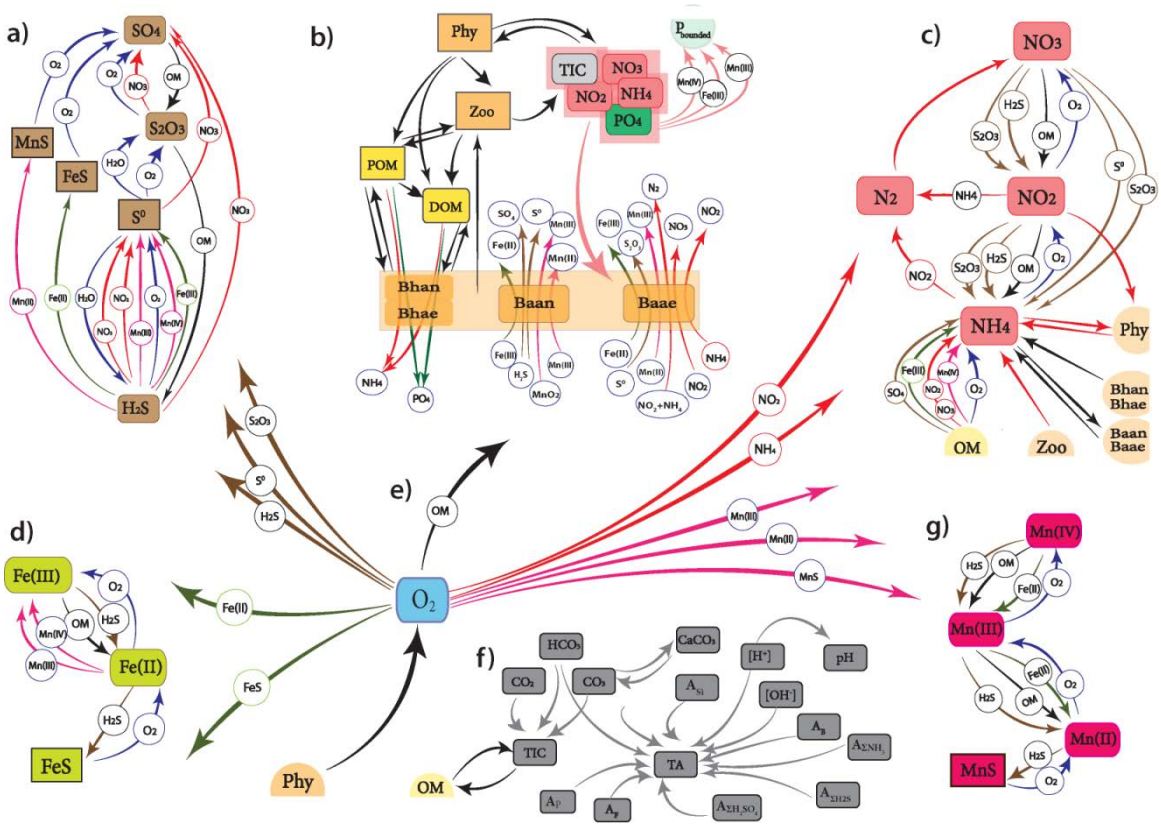

Figure 1. Flow-chart of biogeochemical processes represented in the Benthic RedOx Model (BROM). transformation of sulphur species (a), ecological block (b), transformation of nitrogen species (c), transformation of iron species (d), processes affecting dissolved oxygen (e), carbonate system and alkalinity (f), transformation of manganese species (g).

This work aims to describe the proposed model in a detail and to demonstrate its ability to simulate periodic (seasonal) changes in redox conditions forced by the processes in the water column.

2. Model description

In this study we use the Bottom RedOx Layer Model, BROM, which simulates cycles of C, N, P, Si, O, S, Mn, and Fe to determine redox conditions and the state of the carbonate system across the water column, the bottom boundary layer and the sediments using a one-dimensional vertical transport-reaction model.

The biogeochemical module of BROM is based on ROLM (RedOx Layer Model), which was constructed to simulate basic features of the water column biogeochemical structure in oxic, anoxic and changeable conditions (Yakushev, 2006; Yakushev et al., 2007). ROLM has previously been applied for the description of the water column oxic/anoxic interface structure in the Black and Baltic Seas and the fjords (He et al., 2012; Stanev et al., 2014; Yakushev et al., 2009; Yakushev et al., 2011). A detailed description of ROLM is given in (Yakushev, 2006). We therefore restrict ourselves here to a summary of features. The model includes parameterizations of organic matter (OM) production (via photosynthesis and chemosynthesis) and decay, reduction and oxidation of species of nitrogen, sulfur, manganese, iron, and the transformation of phosphorus and carbon species.

BROM includes a simplified ecological model that considers several principal groups of organisms: phytoplankton, heterotrophic organisms, aerobic autotrophic and heterotrophic bacteria, anaerobic autotrophic and heterotrophic bacteria, as described in (Yakushev et al., 2007).

Compared to ROLM, BROM adds among others a module describing the carbonate system. This is modeled through standard equilibrium assumptions, taking care to account for the dynamic behavior of several components of total alkalinity significant in suboxic and anoxic conditions (i.e. forms of S, N, Mn, Fe).

The physical domain of the model spans the water column, the BBL and the upper layer of the sediments. To parameterize the water column, including temperature, salinity and turbulent diffusivity, we use results of a simulation of turbulent mixing performed with GOTM (Bolding et al., 2001). In the limits of the BBL, mixing was assumed to be constant. In the sediments molecular diffusion and bioirrigation/bioturbation were parameterized.

2.1 Biogeochemical Model.

The following state variables (C_i) were considered in the model (**Table 1**):

A simplified ecological model of BROM, reflects main functional groups of organisms and aims to parameterize the basic features of organic matter production and decomposition. The model is based on the Redfield and Richards stoichiometry (Richards, 1965).

The model contains both frequently measured components (i.e. H_2S, PO_4) with known spatial and temporal variability, and rarely measured variables (S^0, S_2O_3, Mn(III), bacteria). Variables of the latter category were included because their contribution to biogeochemical transformations is believed to be substantial. For instance, bacteria play an important role in many of the processes modelled and can consume or release nutrients as in both the organic and inorganic form. All this predetermines the complexity of the model. The equations and parameters employed in BROM are given in **Table 3**, **Table 4**, **Table 5** , a flow chart of this is shown in **Figure 1**.

In this version of the model, reactions were divided in 2 groups, kinetic processes and protolithic processes, following earlier work (Boudreau, 1996; Jourabchi et al., 2008; Luff et al., 2001). Protolitic reactions are fast compared to the time step. Therefore, equilibrium concentrations of the chemical element species involved in such reactions can be calculated using mass action laws and equilibrium constants for the seawater (Millero, 1995). That takes away the need to include a separate state variable for e.g. pH, which instead is calculated as a diagnostic at every time step. In turn, this pH value is then used to

calculate the chemical equilibrium constants needed to describe the related processes (i.e. carbonate precipitation/dissolution, carbonate system parameters etc.).

Table 1. State variables of the BROM. Concentrations are presented in micromoles for chemical variables and in wet micromoles of nitrogen for biological parameters.

Notation	Name	Dimension
O - oxygen		µM O
O_2	dissolved oxygen	
S - sulfur		
H_2S	hydrogen sulfide	µM S
S^0	total elemental sulfur	µM S
S_2O_3	thiosulfate and sulfites	µM S
SO_4	sulfate	µM S
N - nitrogen		
NH_4	ammonia	µM N
NO_2	nitrite	µM N
NO_3	nitrate	µM N
PON	particulate organic nitrogen	µM N
DON	dissolved organic nitrogen	µM N
P - phosphorus		
PO4	phosphate	µM P
Si - silicate		
Si	dissolved silicon	µM Si
Si_part	particulate silicon	µM Si
Mn - manganese		
MnII	. dissolved bivalent manganese	µM Mn
MnIII	dissolved trivalent manganese	µM Mn
MnIV	particulate quadrivalent manganese	µM Mn
MnS	manganese sulfide	µM Mn
Fe - iron		
FeII	dissolved bivalent iron	µM Fe
FeIII	particulate trivalent iron	µM Fe
FeS	iron sulfide	µM Fe
C - carbon		
DIC	dissolved inorganic carbon	µM C
Alkalinity		
Alk	total alkalinity	µM
Biological parameters		
Phy	phototrophic producers	µM N
Zoo	pelagic and benthic heterotrophs	µM N
Bhae	aerobic heterotrophic bacteria	µM N
Baae	aerobic autotrophic bacteria	µM N
Bhan	anaerobic heterotrophic bacteria	µM N
Baan	anaerobic autotrophic bacteria	µM N

BROM is coupled to FABM, a Fortran-based software framework for coupling hydrodynamic and biogeochemical models (Bruggeman and Bolding, 2014). FABM enables biogeochemical models to be coded once, and then run unmodified in 0D, 1D, 2D and 3D hydrodynamic models (e.g., GOTM, GETM, GLM, MOM, NEMO). FABM's focus lies on modularity of biogeochemical code: complex biogeochemical systems can be modeled as a coupled collection of stand-alone, process- or species-specific modules. The framework itself is a light-weight software component, designed to provide documented interfaces for communication with hydrodynamic and biogeochemical models, to achieve high performance in complex spatial domains (incl. global climate simulation) and to allow maximum

control by end users and scientists through complete run-time configurability: the user can compose an ecosystem model tailored to the region of interest by selecting a subset of relevant biogeochemical modules.
The present version of BROM consists of 3 biogeochemical modules: BROM_bio, BROM_redox and BROM_carb, that can be used in combination with other FABM biogeochemical model (i.e. ERSEM). The 1D BROM transport model is off-line coupled with GOTM for the water column transport process and has its own transport modules for the BBL and upper sediment.

2.1.1 Alkalinity

Total alkalinity, A_T, was a model state variable. Following the formal definition of A_T (Dickson, 1992; Zeebe and Wolf-Gladrow, 2001) the following alkalinity components were considered:

$$A_T = A_C + A_B + A_P + A_{Si} + A_{NH} + A_{HS} + A_F + [OH^-] - [H^+] + A_{OM}$$

The carbonate alkalinity, A_C, the phosphoric alkalinity, A_P, the ammonia alkalinity, A_{NH}, and the hydrogen sulfide alkalinity, A_{HS}, were calculated from the corresponding model state variables according to (Luff et al., 2001, Volkov, 1984). The boric alkalinity, A_B, and the hydrofluoric alkalinity, A_F, were calculated from salinity. Alkalinity connected with organic matter, A_{OM}, was assumed to be 0.

Biogeochemical processes can affect alkalinity via the 'nutrient-H+ compensating principle' formulated by (Wolf-Gladrow et al., 2007): during uptake or release of charged nutrient species, electroneutrality is maintained by consumption or production of proton (i.e. during uptake of nitrate for photosynthesis or denitrification, or production of nitrate by nitrification). This effect was parameterized in the model.

Besides these, the following redox reactions occurring in suboxic and anoxic conditions also affect production or consumption of $[OH^-]$ or $[H^+]$; their effect on alkalinity was explicitly considered in the model:

$4Mn^{2+} + O_2 + \mathbf{4H^+} \rightarrow 4Mn^{3+} + 2H_2O$
$4Mn^{3+} + O_2 + \mathbf{6OH^-} \rightarrow 4MnO_2 + 6H_2O$
$2MnO_2 + \mathbf{7H^+} + HS^- \rightarrow 2Mn^{3+} + 4H_2O + S^0$
$2Mn^{3+} + HS^- \rightarrow 2Mn^{2+} + S^0 + \mathbf{H^+}$
$Mn^{2+} + H_2S \rightarrow MnS + \mathbf{2H^+}$
$4Fe^{2+} + O_2 + 2H_2O \rightarrow 4Fe^{3+} + \mathbf{4OH^-}$
$Fe^{2+} + MnO_2 + \mathbf{4H^+} \rightarrow Fe^{3+} + Mn^{2+} + 2H_2O$
$2Fe^{3+} + HS^- \rightarrow 2Fe^{2+} + S^0 + \mathbf{H^+}$
$Fe^{2+} + H_2S + HCO_3^- \rightarrow FeS + CO_2 + H_2O + \mathbf{H^+}$
$4S^0 + 3H_2O \rightarrow 2H_2S + S_2O_3^{2-} + \mathbf{2H^+}$
$2S^0 + O_2 + H_2O \rightarrow S_2O_3^{2-} + \mathbf{2H^+}$
$4S^0 + 3NO_3^- + 7H_2O \rightarrow 4SO_4 + 3NH_4^+ + \mathbf{2H^+}$
$S_2O_3^{2-} + 2O_2 + \mathbf{2OH^-} \rightarrow 2SO_4^{2-} + H_2O$
$3H_2S + 4NO_3^- + \mathbf{6OH^-} \rightarrow 3SO_4^{2-} + 2N_2 + 6H_2O$
$CaCO_3 \rightarrow Ca^{2+} + CO3^{2-}$

2.1.2 Carbonate system

Equilibration of the carbonate system was considered as a fast process (protolithic reactions). Accordingly, the equilibrium solution was calculated at every time step using the iterative procedure. That was needed to model the fate of, for example calcium carbonate, that are involved in both protolithic reactions and with transport processes. The carbonate system was described using standard approaches (Lewis et al., 1998; Roy et al., 1993; Wanninkhof, 2014; Wolf-Gladrow et al., 2007; Zeebe and Wolf-Gladrow, 2001).

Precipitation and dissolution of calcium carbonate were modeled following an approach of (Luff et al., 2001). The precipitation rate (CO3_prec) was calculated using a linear approximation:

$CaCO3\_prec = k\_caco3\_prec\ (\Omega_{Ca}-1)$

where k_caco3_prec=0.0001 d-1 is precipitation rate, Ω_{Ca} is calcite saturation.

The dissolution rate (CaCO3_diss) was calculated as:

$CaCO3\_diss = k\_caco3\_diss\ (1-\Omega_{Ca})\ CaCO3$

Where _caco3_diss=0.2 d-1 is the precipitation rate, CaCO3 is the calcium carbonate concentration.

2.2 Physical environment

The 1-dimensional model domain spans the water column, the Bottom Boundary Layer (BBL) and the upper layer of the sediments. For actively mixed water columns, the most active zone for the majority of biogeochemical constituents is the upper 10 cm of the sediment. This zone acts as the oxic/anoxic interface, in which dissolved oxygen drops from high values at the sediment surface to zero at depth. If mixing is reduced, in particular in the BBL, the same drop is oxygen is observed higher in the column: the oxic/anoxic interface shifts from the sediments to the water.

For present simulations we consider a water column of 90 m depth, a BBL of 50 cm depth, and a sediment layer of 12 cm depth. This rather thick BBL was taken to illustrate the peculiarities of the biogeochemical structure above the bottom in case of bottom anoxic formation. A bottom anoxic layer of several decimeters thickness can be documented for some regions, for example, the Sea of Azov (Debolskaya et al., 2008). The water column extends from 0 to 90 m (with a spatial resolution of 5 m), the BBL from 90 to 90.5 m (with a spatial resolution of 2.5 cm) and the upper layer of sediments from 90.5 to 90.62 m (with a spatial resolution of 2 mm).

The time space evolution of the BROM biogeochemical variables is described by a system of horizontally integrated vertical diffusion equations for non-conservative substances:

$$\frac{\partial C_i}{\partial t} = \frac{\partial}{\partial z} K_z \frac{\partial C_i}{\partial z} - \frac{\partial (W_C + W_{Mn}) C_i}{\partial z} + R_{C_i} \qquad (1)$$

where C_i - concentration of a model compounds; K_z – vertical transport coefficient; W_C is the sinking rate of the particulate matter; W_{Mn}, - accelerated rate of sinking of particles with settled Mn and Fe hydroxides; $R_{C_i} = \sum_j Rate_{B_j C_i}$ - - combined sources minus sinks of a substance (rates of transformation), being an algebraic sum of terms associated with specific biogeochemical processes ($Rate_{B_j C_i}$).

This canonical water column configuration was primarily designed to provide a hydrodynamic context for biogeochemical process studies. Nevertheless, we use the North Sea data to parameterize water column characteristics and to judge results of the biogeochemical model. Data for water column parameterization include initial profiles of temperature and salinity, external pressure gradients (e.g., tidal constituents), and surface forcing. Data used to judge model results include the fluxes and concentrations in the sediments, as well as additional observations (i.e. local presence of the bacterial mats).

The mathematical parameterization of the vertical exchange treats K_z as the turbulent diffusion coefficient in the water column and molecular diffusion coefficient in the sediments. Bioirrigaion and bioturbation can also be parameterized as modifiers of the value of K_z

To parameterize the water column K_z we used results of simulation of turbulent mixing in the Northern North Sea performed with the General Ocean Turbulence Model (GOTM) (Bolding et al., 2002)

http://www.gotm.net/index.php?go=software&page=testcases. From initial profiles of temperature and salinity, time-varying surface forcing and external pressure (tidal constituents) GOTM calculates seasonal and depth-varying values of the turbulent kinetic energy and dissipation rate, which in turn are used to estimating the value of K_z throughout the water column. We are aiming for a solution representative for "present day", and we are thus treating the GOTM setup incl. forcing as representative for a "normal year"

For the BBL K_z was assumed to be constant with value 0.5 10^{-6} m^2s^{-1}.

In the sediments, K_z was parameterized as a sum of the pore water molecular diffusion coefficient K_{z_mol}=1 10^{-11} m^2s^{-1} and bioirrigation/bioturbation coefficient.

2.3 Bioturbation/bioirrigation

Bioturbation activity (i.e. mixing of sediment particulates by burrowing infauna) and bio-irrigation (i.e. flushing of benthic sediment by burrowing fauna through burrow ventilation) were parameterized in the model. In mesocosm experiments with North Sea sediments (Queirós, 2014) the biodiffusion coefficient was found to be 2 - 5 cm^2yr^{-1} (0. 6 – 1.6 10^{-11} m^2 s^{-1}) and the maximum bioturbation depth was 0.5-2.2 cm, with higher values in natural conditions. Since in the model we aim to parameterize the combined effect of bioturbation and bioirrigation, we assumed a constant $K_{z\_bio\_max}$ = 1.10^{-11} m^2 s^{-1} in the upper 2 cm, followed by exponential decrease with increasing sediment depth. A dependence of Kz_bio on oxygen was introduced to parameterize the absence of bioturbation/bioirrigation in case of anoxia.

$$K_{z\_bio} = K_{z\_bio\_max} \frac{O_{2s}}{O_{2s}+K_{O2s}} \qquad (2)$$

where O_{2s} is the concentration of dissolved oxygen at the sediment surface, $K_{z\_bio\_max}$ is maximum bioturbation/bioirrigation coefficient and K_{O2s}= 1 µM is a constants.

2.4 Particle sinking

Constant W_{Ci} values were assumed for phytoplankton, zooplankton, bacteria, and detritus (**Table 4**). In addition, the effect of increased sinking rates due to the formation of Mn(IV) and Fe(III) oxides and their association with particulate organic matter (POM) was parameterized. It was found that the precipitation of particulate Mn oxide significantly increases the flux of sinking particles, which, in turn, affects the overall distribution of particles (Yakushev and Debolskaya, 1998). This effect was parameterized in the following equation as an additional term reflecting this effect:

$$W_{Me} = W_{Me}^{\max} \frac{Mn(IV)}{Mn(IV)+K_{Me}} \qquad (3)$$

Coefficients W_{Me}^{max} and K_{Me} are given in **Table 5**.

2.5 Boundary Conditions

The water column area considered in our model spans everything between the sea surface (upper boundary) and at 15 cm depth of the sediments (lower boundary). At the upper boundary, the surface fluxes of the modeled chemical constituents are assumed to be zero, with the exception of O_2, CO_2, PO_4, inorganic nitrogen compounds and Fe and Mn oxides.

For oxygen, the surface flux represents exchange with the atmosphere. This is given by the flux equation:

$$Q_{O_2} = k_{660}\,(Sc/660)^{-0.5}\,(Oxsat - O_2)\,, \qquad (4)$$

where *Oxsat* is equal to oxygen saturation as a function of temperature and salinity, according to UNESCO (1986); *Sc* is the Schmidt number; k_{660} is the reference gas-exchange transfer velocity (*Sc* = 660, CO_2 at 20°C). To describe k_{660} as a function of wind speed, the following equation is used:

$$k_{660} = 0.365\ u^2 + 0.46\,u\,. \qquad (5)$$

Simulations are carried out using a mean wind speed of 5 m s^{-1}.

CO_2 exchange was parameterized in a same way as for oxygen, with atmospheric CO_2 equal 400 ppm during all the seasons.

Inputs of phosphorus, nitrogen, iron and manganese from atmospheric precipitates and rivers were taken into account by prescribing concentrations at the sea surface. For phosphorus (Q_P) and nitrogen (Q_N), the seasonality in these inputs was considered by imposing time-varying surface concentrations:

$Conc(PO_4)=(1+\sin(2\pi*(julianday+55)/365))*0.9$

$Conc(NO_3)=(1+\sin(2\pi*(julianday+55)/365))*7.$

where julianday is the Julian day number.

Constant surface concentrations were prescribed for the following variables: SO_4 (25 10^{-3} µM), DIC (2100 µM), Alk (2250 µM), Mn(IV) (1x10^{-4} µM), Fe (III) (5x10^{-5} µM). At the lower boundary we assumed a constant concentrations of SO_4 (25x10^{-3} µM). Therefore, the model biogeochemistry was predominantly forced by the upper boundary conditions; the concentrations at the lower boundary emerge as a result of processes occurred in the water column, BBL and upper sediment.

2.6 Computational aspects

Numerical integration was conducted with the Eulerian scheme and by process splitting (i.e., separate treatment of diffusion, advection/sinking and reaction/source-sink terms). Time steps were set to 0.0005 d for diffusion and 0.001 d for biogeochemical processes and sinking. The initial calculations assume a vertically homogenous distribution of all biogeochemical variables, with compound-specific initial concentrations. To subsequently resolve spatial and temporal variation in the biogeochemical components, calculations are repeated with seasonal changes of temperature, salinity, vertical turbulence in the water column (calculated with GOTM) and irradiance until a quasi-stationary solution with seasonal forced oscillations of the biogeochemical variables is reached. The code is written in FORTRAN and was run with the Intel FORTRAN for Windows Compiler.

To determine the vertically balanced distribution, the calculations were repeated with seasonal changes of temperature, salinity, vertical turbulence in the water column (calculated with GOTM) and irradiance until a quasi-stationary solution with seasonal forced oscillations of the biogeochemical variables was reached. There were no changes in the year-averaged concentrations of the variables for at least 100 model-years.

3. Results

Here we present model results for the seasonal variability of biogeochemical variables, emerging from the interplay of modelled biogeochemical processes, the variability in environmental conditions (temperature, salinity, turbulent mixing), and the imposed boundary conditions (prescribed constant concentrations for selected variables).

3.1 Dissolved oxygen, nutrients, sulfur and metals

At the end of the winter period (day 90, **Figure 2**) intense turbulent mixing occurred throughout the water column, leading to uniform vertical distributions of temperature and salinity. During this period, oxic conditions prevail throughout the water column and the BBL, with oxygen concentrations decreasing from 300 μM in the surface layer to 170 μM at the sediment–water boundary. Due to bioturbation the few upper millimeters of the sediment were also oxygenated. Nitrate concentrations increased to the bottom of the water column, reaching about 13 μM near the sediment surface then dropping to negligible values over the upper millimeters of the sediments, directly following the disappearance of O_2. The nitrite peak (5 μM) was positioned below the sediment surface, and deeper in the sediment nitrogen was present in the form of ammonia, which increased to about 280 μM at 4 cm depth of sediments and remained constant in the deeper layers.

According to the model scenario, Mn concentrations were assumed to be constant with time at the sea surface. The concentrations within the water column were small because Mn(IV) formed under oxic conditions precipitated to the bottom where it reduced due to reactions with OM and reduced species of Fe and S. The calculated distributions show a maximum of Mn(IV) directly at the sediment water interface (20 μM), followed by a Mn(III) maximum in the upper millimeters of the sediment (6 μM) and the Mn(II) maximum at about 5 mm depth (20 μM). In the deeper layers Mn(II) concentrations decreased to 15 μM, while concentrations of MnS increased to 3 μM.

The distributions of Fe species were similar to those of Mn. The concentrations in the water column were very low due to precipitation of Fe(III). The upper millimeters of the sediment were enriched with Fe(III) to 13 μM. A maximum (12 μM) of Fe(II) was positioned below, and in the deeper layers the dominant form of Fe was FeS (reaching 9 μM).

Phosphate had a uniform distribution in the water column (about 1-2 μM). In the sediments its concentration first increased to 16 μM, followed by a minimum coinciding with the lower part of the Mn(III) maximum. In the deeper layers its concentrations increased again, reaching 21-22 μM at 12 cm depth.

H_2S first appeared at 7-8 mm depth, coinciding with depletion of Mn(IV), Mn(III) and Fe(III). H_2S concentrations increased in the upper 4 cm of the sediment to about 150 μM and remained constant in the deeper layers. The reduced sulfur intermediates, S^0 and S_2O_3 first appeared at the sediment surface. The S^0 distribution was characterized by a maximum (35-40 μM) at about 1-3 cm sediment depth, after which its concentration decreased to the low boundary of the model. Concentrations of S_2O_3 increased with depth reaching about 90 μM at 5 cm depth, and then remained constant.

With the water column about to undergo stratification, the distributions of biological parameters corresponded to the beginning of spring: the maximum Phy concentrations were at the sea surface, the heterotrophs, Zoo were found both in the surface layer and in the bottom layer. Aerobic heterotrophic bacteria dominated in the water column, anaerobic heterotrophic bacteria were found in the upper millimeters of the sediment. Maxima in aerobic and anaerobic autotrophic bacteria were found practically at the same depths just below the sediment-water interface.

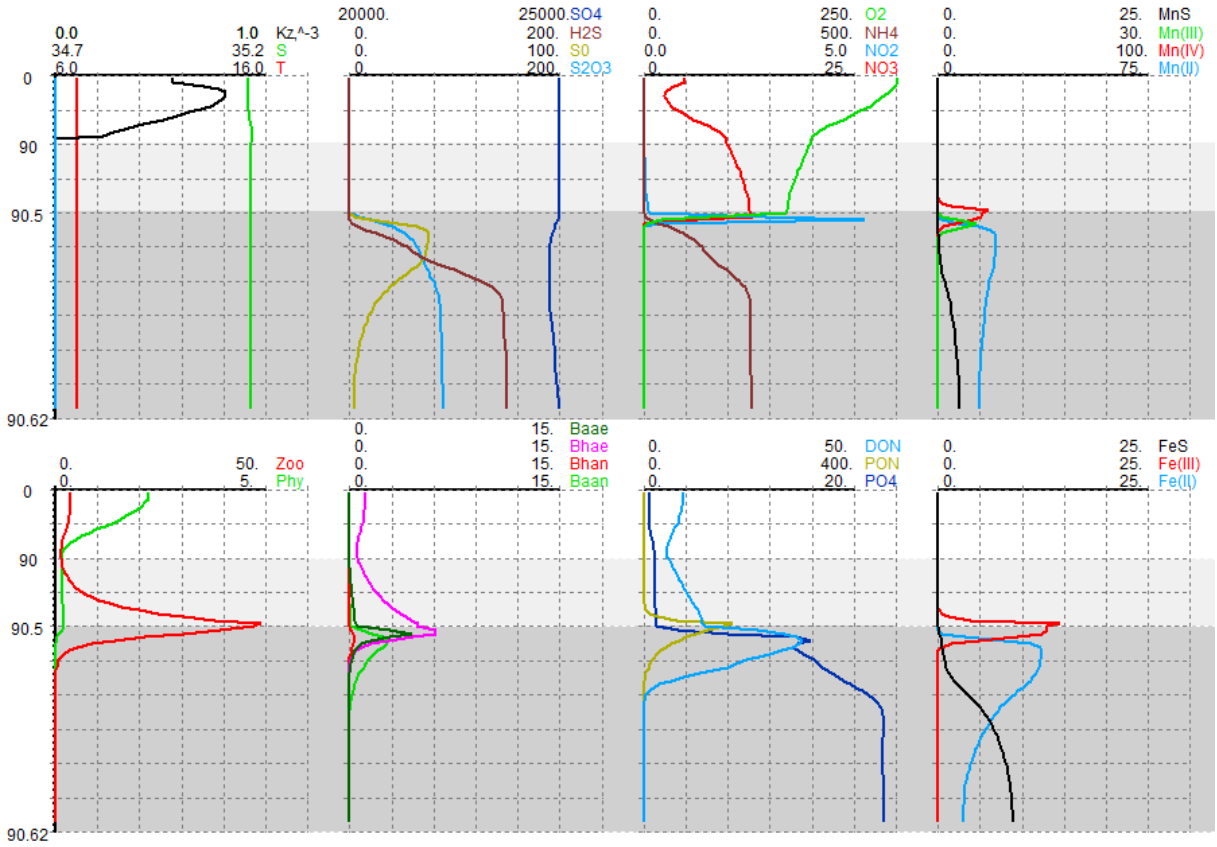

Figure 2. Vertical distributions of the modelled chemical parameters (µM), biological parameters (µM N), temperature (°C), salinity (PSU) and vertical transport coefficient ($10^{-3}m^2s^{-1}$) in winter well-mixed conditions (day 90) in the water column 0-90 m (white background), the 50 cm thick BBL (90-90.5 m , light grey background) and 12 cm upper sediment pore water (90.5-90.62, dark grey background).

In the summer period (day 215, **Figure 3**) a thermocline has formed, connected with the summer warming. Decrease of the surface salinity also contributed to the formation of a halocline positioned at the same depth. That leads to a decreased vertical mixing in the vicinity of the formed pycnocline. After the phytoplankton bloom and pycnocline formation, the bottom waters were characterized by an increased amount of particulate and dissolved OM and restricted flux of oxygen from the surface layer that lead to intensive oxygen depletion. The profiles shown in **Figure 3** demonstrate that the drop in oxygen concentration now happens within the water. Additionally, we can observe a suboxic zone, with an absence of both oxygen and hydrogen sulfide. H_2S was absent at the sediment water interface, because the oxidative forms of Fe and Mn were still present in the sediments and oxidized H_2S inside the sediments. Meanwhile, intermediate reduced species of sulfur, S_2O_3 and S^0 were released into the water.

Nitrate was consumed near the bottom for denitrification and there was formed a nitrate maximum (24 µM) above the BBL, followed by a nitrite maximum (0.8 µM) below. The concentration of ammonia increased in the upper centimeters above the bottom (reaching 5 µM near the sediment-water interface). Modelled PON and DON had maxima at the surface in 1 cm depth respectively, and depleted deeper. The model fate of the OM corresponds to the classical ideas that the major part of the OM produced in the surface waters (about 99% in the oligotrophic ocean, is decomposed before being buried below the depth of bioturbation (Boudreau, 1996; Canfield et al., 1993).

Mn(III), Mn(II) and Fe(II) were also present in detectable concentrations in the bottom water. Phosphate concentrations increased at the sediment surface to 10 µM, and a subsurface minimum present in winter (**Figure 4**) now was absent (**Figure 3**).

Concentrations of the living organisms in this period reach their annual maximum values. An increase of particulate and dissolved organic matter leads to the growth of both aerobic and anaerobic heterotrophic bacteria. Aerobic and anaerobic autotrophic bacteria were found both below the sediment/water interface and in the lower centimetres above the sediments, testifying to a formation of bacterial mats typical for the oxygen depleted bottom areas.

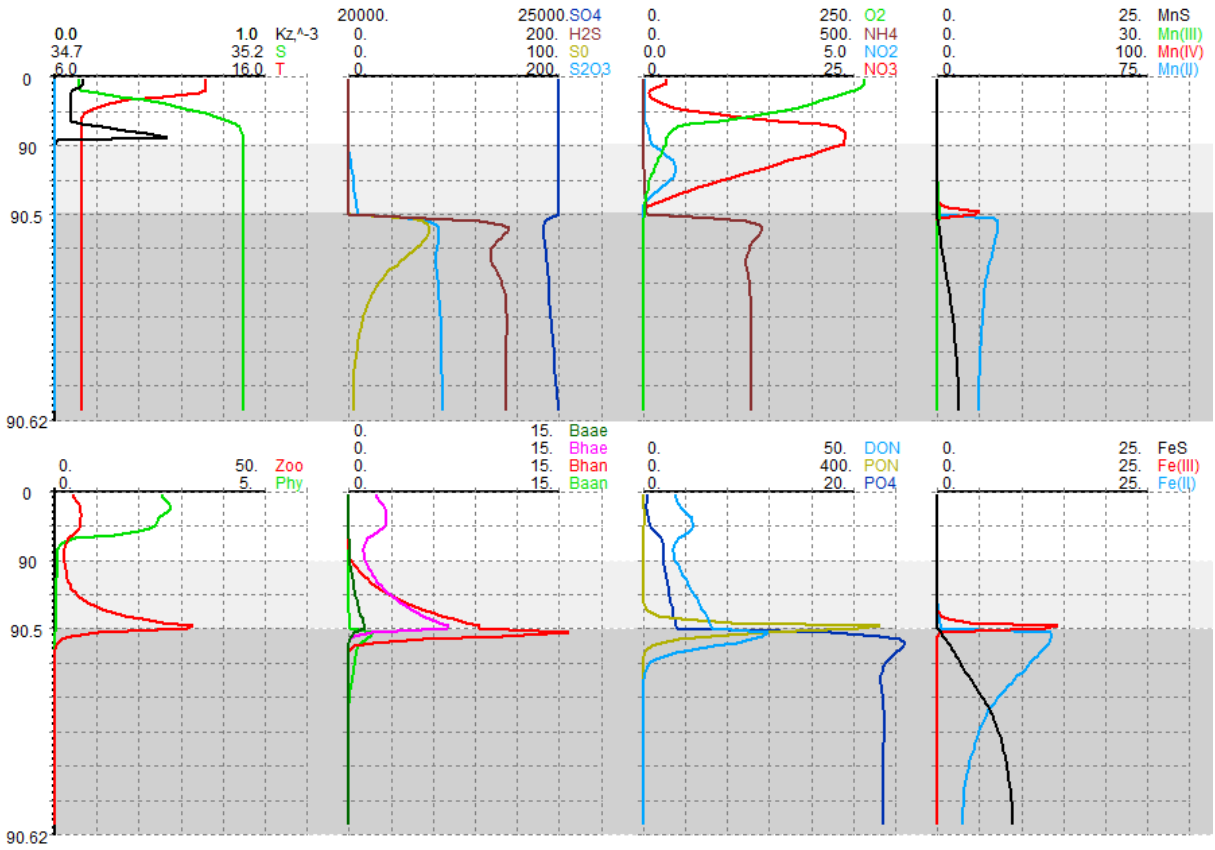

Figure 3. Vertical distributions of the modelled chemical parameters (µM), biological parameters (µM N), temperature (^{o}C), salinity (PSU) and vertical transport coefficient ($10^{-3}m^2s^{-1}$) in the period of organic matter production and formation of pycnocline (day 215).

In the stagnation period (day 300, **Figure 4**) the vertical gradient of temperature reached its maximum value and the water column pycnocline restricted the supply of oxygen to the deep. In the bottom layer, Mn and Fe oxides deposited earlier at the sediment surface were completely reduced, and H_2S had penetrated into the bottom water. Reduced sulfur intermediates, S^0 and S_2O_3 as well as Fe(II) and Mn(II) were also found in the bottom water. Maximum of nitrate and nitrite were positioned in the upper layers, and there were no available oxidizers at the sediment water interface save sulfate and carbon dioxide. The simulated model distributions in the water column correspond well to the principal features of the water column redox interfaces structure, as observed in the Black Sea, the Gotland Deep and other regions (Kamyshny et al., 2013; Yakushev et al., 2007).

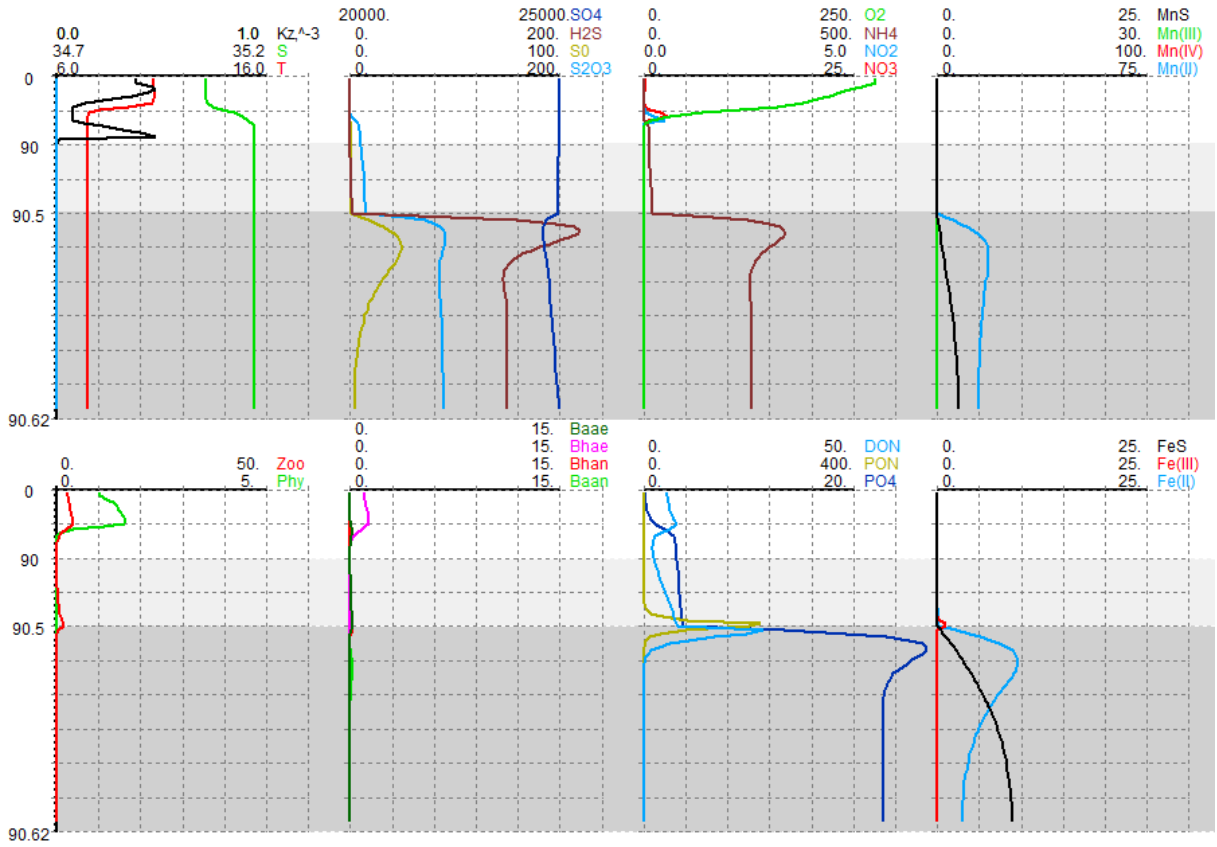

Figure 4. Vertical distributions of the modelled chemical parameters (µM), biological parameters (µM N), temperature (°C), salinity (PSU) and vertical transport coefficient ($10^{-3}m^2s^{-1}$) in the period of stagnation and bottom anoxia (day 300).

3.2 Carbonate system

The results of the baseline simulations of the carbonate system parameters are shown in **Figure 5**.

In the upper water layer pH values are high (8.10 in winter and 8.23 in summer), the values of pCO2 are close to the equilibrium with the atmosphere (about 400 ppm), calcium carbonate is oversaturated (about 2.5 for aragonite and about 3.5 for calcite. The values of Alk (2300 µM) and DIC (2200 µM) are close to the typical for the Ocean.

In the seasonally anoxic deep water layer and BBL pH oscillated from 7.6 in oxygenated period to 7.3 during anoxia. pCO2 varies from to 500-600 ppm to 1500-1700 ppm. Aragonite and calcite saturations change from 1 and 1.5 in oxic conditions to 0.4 and 0.5 in anoxic conditions, respectively.

Alkalinity and DIC take on smaller values in oxic conditions (2200-2300 µM and 2200 µM) and larger values during anoxic conditions (2400 µM and 2500 µM).

In the upper 12 cm of the sediment pH is about 7.1 and pCO_2 is about 5300 ppm. A local pH maximum in the upper millimeters of the sediment in the period before the bloom is connected with chemosynthesis that leads to intensive CO_2 consumption (**Figure 5**, top). In the summer period and the period of stagnation, we find instead a pronounced pH minimum in the upper layer of the sediment connected with sulfate reduction intensification (**Figure 5** middle and bottom). The BBL and the top few mms of the sediment are oversaturated with respect to aragonite and calcite during the oxygenated period and precipitation of $CaCO_3$ occurs, while during the anoxic period this $CaCO_3$ dissolves.

The performed calculations show that in natural conditions there might be significant season variations in the BBL of the carbonate saturation values, and pH. Modelled $CaCO_3$ concentrations vary in a course of year with the maximum values of 0.5 mM at March and minimum<0.1 at summer and autumn (**Figure 5**).

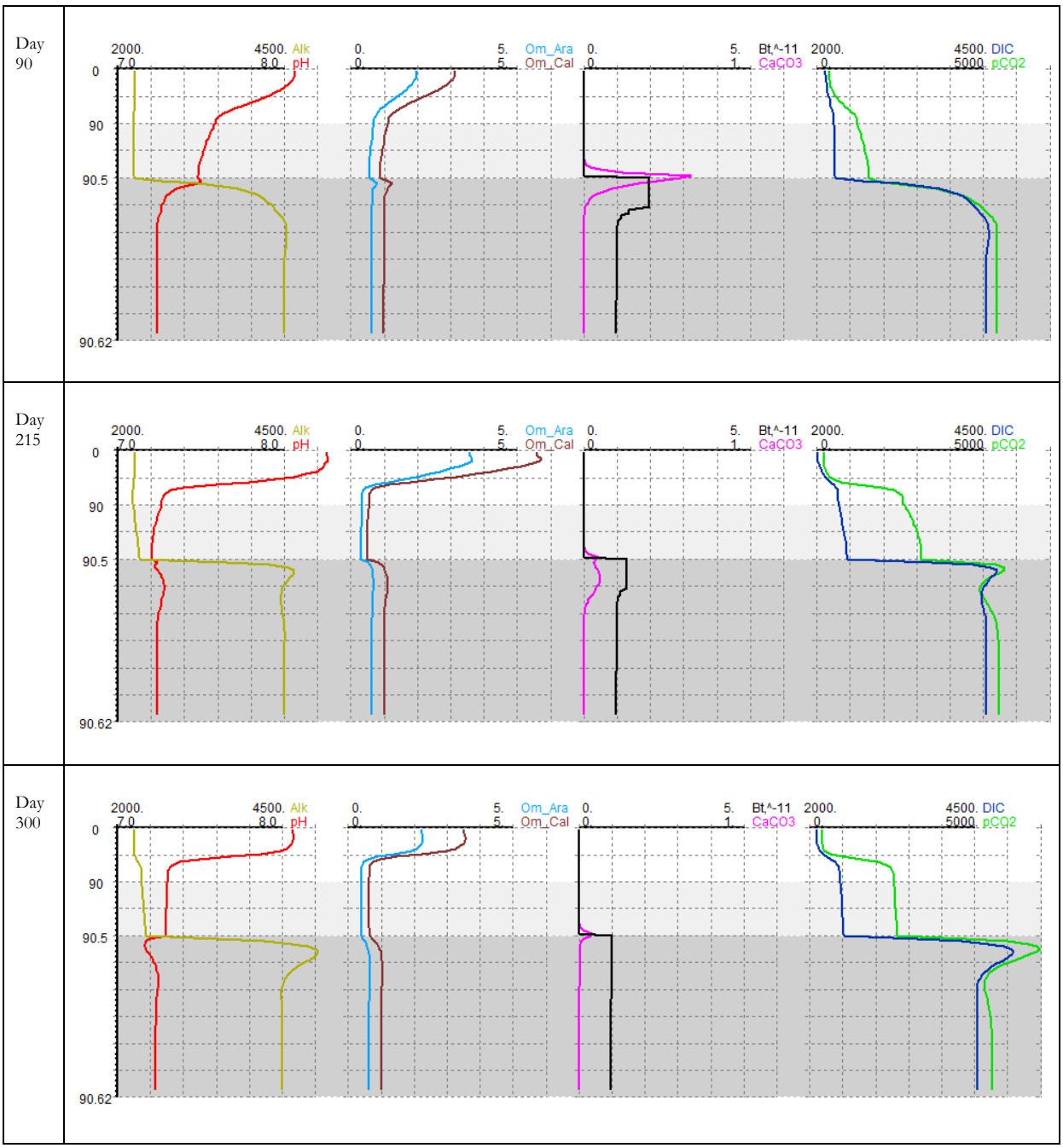

Figure 5. Vertical distributions of the modelled carbonate system parameters in the winter well-mixed conditions (day 90), in the period of organic matter production and formation of pycnocline (day 215) in the period of stagnation and bottom anoxia (day 300).

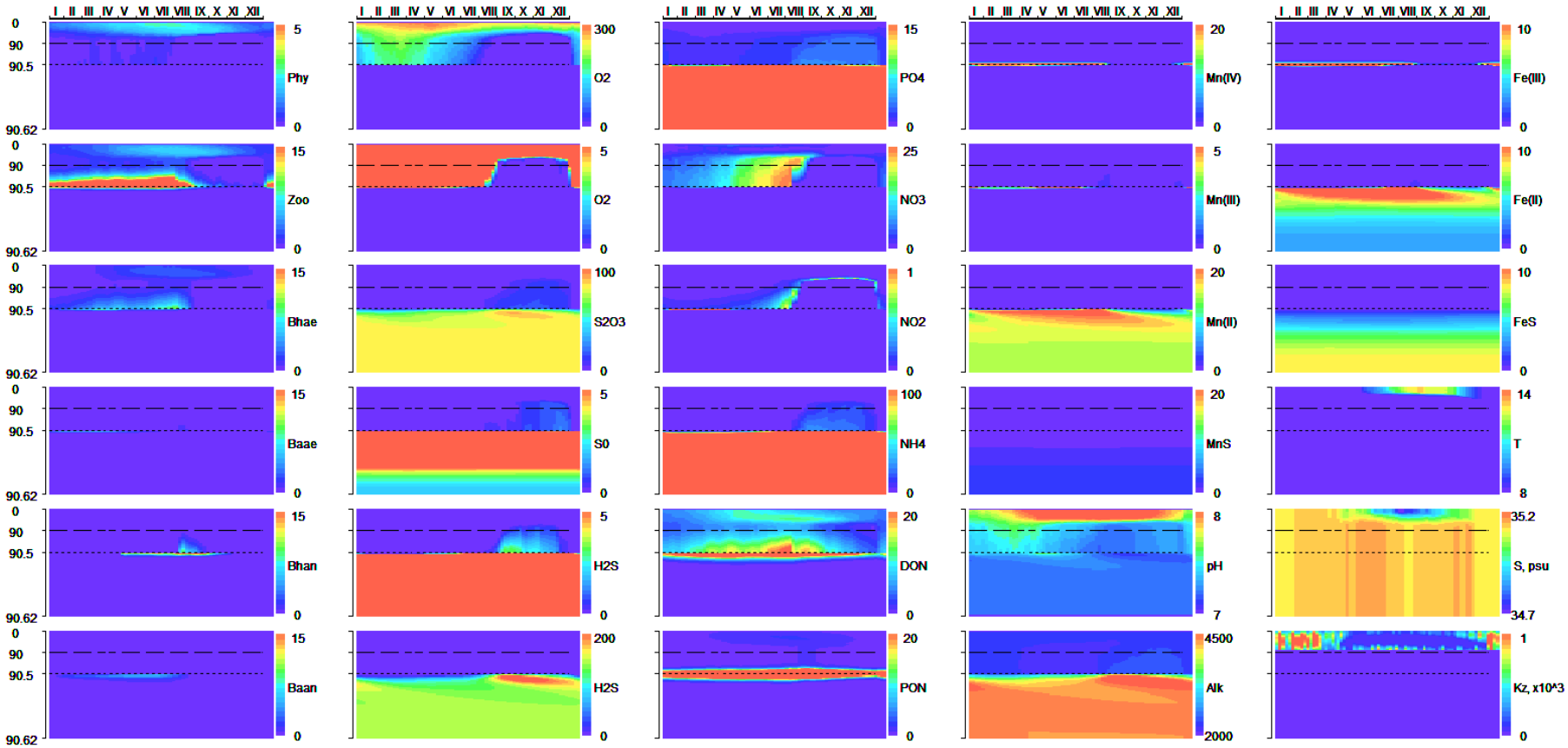

Figure 6. Simulated seasonal variability of the modelled chemical parameters (µM), biological parameters (µM N), temperature (oC), salinity (PSU) and vertical transport coefficient ($10^{-3}m^2s^{-1}$). The dotted line corresponds to the sediment-BBL boundary and the dashed-line to the BBL-water column boundary.

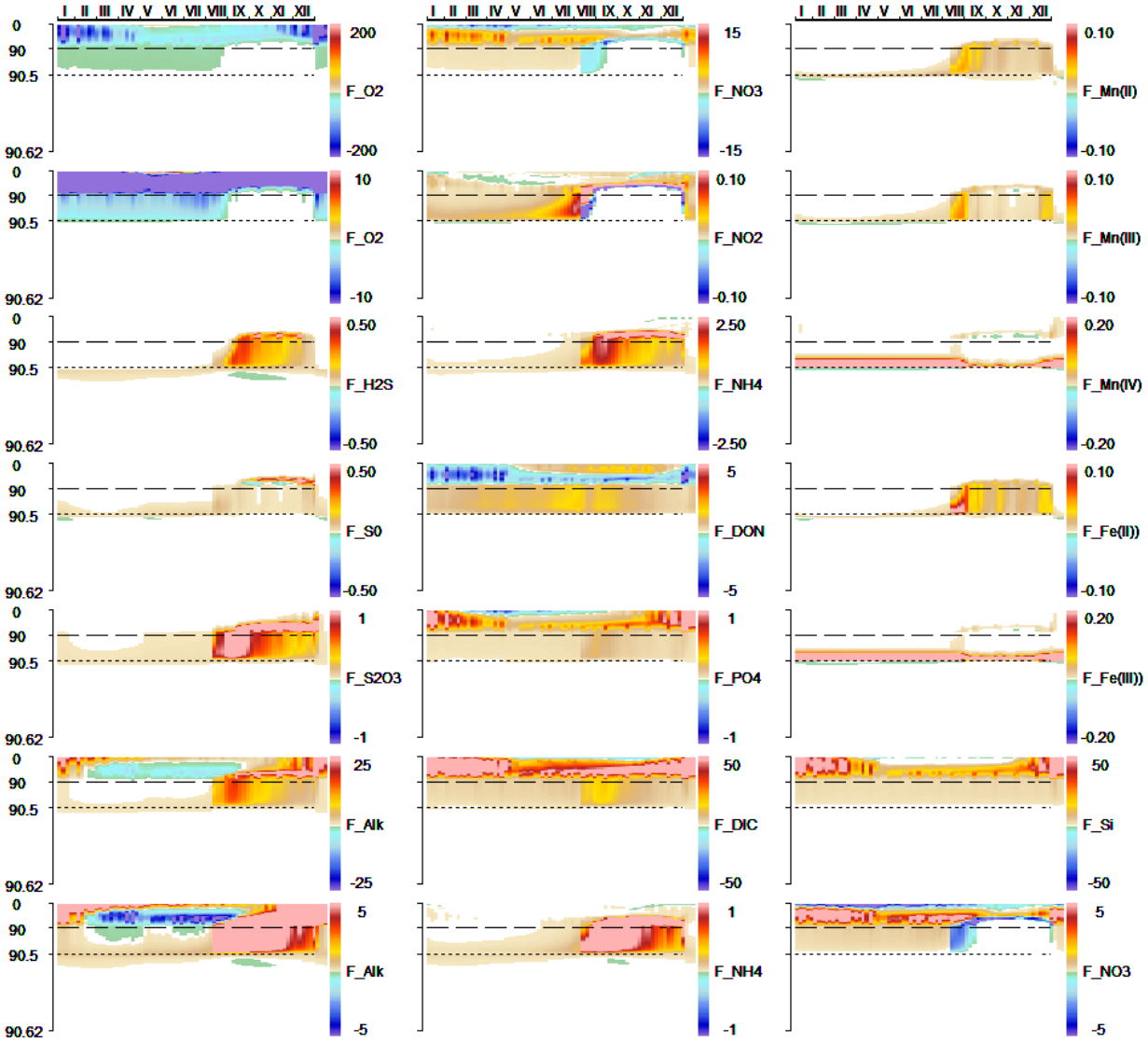

Figure 7. Simulated seasonal variability of vertical fluxes of oxygen, nitrate, Mn(IV), Mn(III), Fe(III), hydrogen sulphide, phosphate, ammonia, thiosulfate and elemental sulphur in mmol m^2 d^{-1}.

4. Discussion

The calculations performed allowed to demonstrate the capability of the BROM: (i) to reproduce seasonal variation in oxygen concentration and redox state, (ii) to resolve fine scale structure of the column in BBL and sediment, (iii) to capture the time lags associated with rarely modelled compounds (e.g., Mn and Fe oxides role in securing of the H2S efflux from the sediments after complete oxygen consumption).

In this work we used a simplified hydrodynamic scenario, since the main goal of the model was to reproduce the biogeochemical mechanism of transformation of oxic conditions into anoxic in the sediment-water interface. The model biogeochemical modules consider relatively fast processes, (seasonal and shorter), and therefore the processes parameterized did not cover all the processes occurring in the sediments (they exclude longer time scale processes, occurring on e.g. geological time scales). Additionally, the model was forced only from the upper and did not include fluxes of reduced components (i.e. hydrogen sulfide, Mn(II), MnS, FeS) across the bottom of the sediment layer, in order to focus exclusively on the consequences of supply of the fresh organic matter as a main reducer in the water column and in the sediments.

The simulations revealed some principle features of the sediment water interface biogeochemistry. First of all, the model shows a possibility of the periodic replacement of oxic conditions with anoxic, which leads to changes in the vertical distributions of the biogeochemical variables and their fluxes. The forms of the model chemical elements N, Fe, Mn, S varied spatially from oxic in the water column to anoxic in the sediments, and varied temporally in the BBL.

To get further insight into the temporal variability of different variables, simulated seasonal changes between the oxic and anoxic vertical distributions are shown in **Figure 6** and between normoxic and anoxic vertical fluxes in **Figure 7**

In the model, the oxic/anoxic interface was positioned at several millimeters depth in the oxygenated winter period (**Figure 2**). Deposition of large amounts of OM at the bottom under restricted oxygen supply lead to a shift of this interface toward the sediment surface, due to consistent consumption of O_2, NO_3, Mn(IV), Mn(III), Fe(III) and SO_4 for the OM mineralization (**Figure 4**). In the limits of the BBL O_2 started to disappear in the middle of summer, accompanied by slower remineralization of OM and slower oxidation of reduced forms of Mn, N, Fe and S. After O_2 consumption, NO_3 became a dominant oxidizer, which was then also rapidly depleted.

The model simulations show that after the decrease of oxygen at the sediment-water interface to 5 μM, the release from the bottom of S_2O_3 and S^0 starts, while hydrogen sulfide initially remains in the sediments and enters the water column several days later. This is explained by thesignificant concentrations of Mn and Fe oxides in the upper millimeters of the sediments which prevented the immediate release of H_2S. Mn and Fe oxides react with hydrogen sulfide producing S_2O_3 and S^0. The order of appearance in the water columnof the intermediate sulfur species (first S_2O_3, than S^0 and than H2S) corresponds to their typical order of appearance at the water column redox interfaces (Kamyshny et al., 2013). The delayed release of H2S allowed the bottom surface and the BBL to be in suboxic conditions, allowing the accumulation of Mn(III).

Disappearance of the oxidized forms of Mn and Fe resulted in a sudden increase in concentrations of H_2S as well as phosphate, which was also "trapped" by Mn and Fe oxides. The calculated seasonal variability of the vertical fluxes () illustrates this behavior and allows us to compare roles of different species affecting the position of the redox interface.

The dissolution of Fe and Mn oxides in late summer leads to a release of the H_2S from the sediments and an upward shift of the oxic/anoxic interface into the water column (**Figure 6**). This is accompanied by

the disappearance of the phosphate minimum at the sediment surface (connected with trapping by the metal oxides) and sudden influx of phosphate from the sediment into the water.

During the anoxic period, transport fluxes of hydrogen sulfide, manganese (II), phosphates, Fe(II),S_2O_3 and NH_4 are upward (**Figure 7**).

The majority of occurring redox processes are microbially dominated, leading to bacterial growth (both heterotrophs and autotrophs) and production of new OM (by autotrophs). This forms a positive feedback that accelerates the consumption of oxidizing compounds.

After the formation of suboxic and anoxic conditions in the BBL, aerobic heterotrophic bacteria disappear, and an increase of the aerobic autotrophic and anaerobic heterotrophic bacteria is seen. This increase of the bacterial concentrations at the sediment surface corresponds to the presence of bacterial mats which mark out the local spots of hypoxic/anoxic conditions.

Winter flushing events lead to an abrupt increase of O_2 above the bottom, the appearance of Mn(IV), Mn(III) and Fe(III) in the water column, and their accumulation at the sediment surface. This is followed by a deepening of the oxic /anoxic interface inside the sediments during the winter.

The model clearly demonstrates the presence of a fine vertical biogeochemical structure in the limits of BBL (**Figure 2**, **Figure 3**, **Figure 4**). That means that the concentrations and fluxes change over every cm of the water boundary layer and also temporally during the year. This should be taken into account while analyzing the data of observations and experiments, since the methods applied usually don't allow for fine-structure sampling. For example, in the standard methods of the sediment –water flux measurements with the box corers or benthic chambers, this fine structure is destroyed.

4.1 Comparison with data

Validation of the present complex multi component model against data is far from trivial, because it is practically impossible to measure all the model components at a vertical and temporal resolution that does justice to the rapid temporal variation and fine scale vertical structure seen in the model results.

For our North Sea water column scenario, we can compare its results against the data collected in the Sleipner area during the projects FP7 ECO2, FP7 RISCS, FME SUCCESS and CO2Base during the studies of the BBL. Besides this, we can use the literature data on typical values or distributions collected in the other regions.

The values and ranges of changes of the chemical elements and values of the fluxes for the parameters with available data are the following.

4.1.1 Dissolved oxygen.

The model reproduces changes of oxygen concentrations at the sediment-water interface from 200 μM in oxygenated period to 0 μM during the anoxia. The field data in the Sleipner area show DO oscillations from 160 to 360 μM in the bottom water during the 2 months period observations (Linke, 2014). The modeled downward vertical flux of oxygen was found to the highest in the water column below the euphotic zone in winter and early spring, it and sporadically exceeds 200 mmol m^{-2} d^{-1}, in connection with the mixing intensity changes (**Figure 6**, **Figure 7**). In the limits of the BBL oxygen flux decreases from about 10 to 0 mmol m^{-2} d^{-1}, corresponding to the typical values of the oxygen flux that can be received in the field and laboratory experiments. For example, during the chamber experiments there was measured sediment oxygen consumption in the range 3.9-4.6 mmol m^{-2} d^{-1} in the Sleipner area. (Queirós, 2014).

The sediment pore water profile measured during the laboratory experiment shows that oxygen depletes at 9 mm depth in oxic conditions and 3 mm depth in hypoxic (Queirós, 2014), that corresponds well to the modeled distribution in oxic conditions (**Figure 2**).

Actually the mentioned field and experimental data were collected in the background area with oxic conditions, while the model can describe the biogeochemistry of the bottom areas with the restricted aeration, i.e. trenches and methane sips where hypoxia and anoxia can occur.

The model predicts disappearance of oxygen in the sediments, and in the near-bottom water during the stagnation period (**Figure 3**, **Figure 4**)

4.1.2 Nitrogen

In the oxic period the modelled water column nitrate corresponded to the climatic values (i.e. http://www.nodc.noaa.gov/). In the sediments the modelled nitrogen was represented by ammonia with concentrations 250 µM, that is 2 times higher than measured during the experiments (120 µM) (Queirós, 2014).

The flux of NO3 changed its direction (**Figure 7**). In oxic conditions an upward flux of nitrate exists in the limits of the BBL and in the water column, compensating the loss of nitrate for photosynthesis production. In suboxic conditions there is a downward flux of nitrate connected with denitrification.

The modelled upward values of the nitrate flux in the BBL – 0.5 -2 mmol m^{-2} d^{-1} in oxic period are within the range of measured values (from -0.5 to 2.5 mmol m^{-2} d^{-1}) (Queirós, 2014)

The flux of ammonia is directed upward throughout the year, and changes from 0.03 mmol m^{-2} d^{-1} during the oxic period to more than 1 mmol m^{-2} d^{-1} during the anoxic period. The measured ammonia flux was in the range from -1 to 3 mmol m^{-2} d^{-1} (Queirós, 2014).

4.1.3 Phosphorus

The modelled concentrations of phosphate increased from 0-2 µM in the the water column to around 4 µM in the BBL, which is higher than typical measured values.

Modelled phosphate concentrations in the sediments (20-23 µM) were higher than the measured values of around 5 µM (Queirós, 2014). Modelled phosphate fluxes in the BBL were less than 0.01 mmol m^{-2} d^{-1} in oxic conditions, increasing to 0.01 mmol m^{-2} d^{-1} in anoxic; these are comparable with measured values ranging from -1 to 0.9 mmol m^{-2} d^{-1} (Queirós, 2014).

4.1.4 Manganese

In oxic conditions manganese content was negligible in the water column and the sediment-water interface was characterized by an accumulation of Mn(IV). Beneath the modelled maximum of Mn(IV) a peak of Mn(III) is formed, followed by a Mn(II) maximum and finally by a MnS increase, in agreement with the modern paradigm of Mn species distributions in the sediments (Madison et al., 2013).

But from qualitative point of view the modelled Mn(II) concentrations in the sediments (15 µM) were much lower than obtained in experiments (over 100 µM,(Queirós, 2014). This is connected with the model assumption of an absence of any forcing from the lower boundary, such that all the Mn inventory in the model was formed by a weak flux from the surface.

The model predicted the observed small concentrations of Mn(III) and Mn(II) in the bottom water during the stagnation period, but the modelled concentrations of Mn(II) were much smaller than observed . Modelled fluxes of Mn(IV),Mn(III) and Fe(III) were negligible (less than 0.01mmol $m^{2}d^{-1}$) while the measured fluxes varied from -3 to 20 mmol m^{-2} d^{-1} (Queirós, 2014).

4.1.5 Iron

The distributions and variability of iron species were similar to those of manganese. As for Mn(II) the maximum modeled concentrations of Fe(II) (about 3-7 μM) were much smaller than measured (over 50 μM) (Queirós, 2014).

The distributions of modelled concentrations and fluxes listed above reflect the principal features of their observed variability. Quantitative discrepancies in the pore water concentrations were likely connected with the absence of forcing from the lower boundary. This may explain the lower concentrations of metals in the model, while the higher concentrations of nutrients (N and P) may result from excessive fluxes from the surface, needed to feed the model with enough OM content for anoxia formation demonstrations. Regarding an allocation for the North Sea scenario all these discrepanciescould potentially be improved, given adequate data, by the introduction of forcing from the lower boundary and a better representation of the upper boundary.

4.2 Carbonate system

The modelled distributions of carbonate system parameters and their variability and fluxes are shown in **Figure 5**, **Figure 6**, **Figure 7** .The ranges of the concentrations for all three model' media were discussed above. Here we focus on the influence of periodic anoxia formation in the BBL and the upper layer of the sediments on the carbonate system.

The processes connected with changes of redox conditions represent an important factor of influence on the carbonate system and alkalinity. For example, pH dynamics caused by OM degradation are modulated by pH buffering due to precipitation and dissolution of carbonates (Luff et al., 2001), sulphate reduction producing large amount of bicarbonate-ion (Boudreau, 1996), Mn reduction increasing alkalinity by producing bicarbonate and consuming protons (Sternbeck, 1995), and Fe reduction leading to a consumption of a proton (Luff et al., 2001). The model allows a quantitative analysis of how these processes (and some others, i.e. chemosynthesis) interact and combine. During the work on model it was possible to "unlock" certain processes and to demonstrate their specific significance.

The received results are the following. In the BBL water pH oscillated from 7.6-7.7 in oxygenated period to 7.2 in the beginning of stagnation with a slight increase to 7.3 in the developed stagnation (**Figure 5**). Alkalinity and DIC increases from about 2250 μM during the oxic period to 2350-2450 μM and 2450-2500 μM respectively during the anoxic period. pCO2 changes from 700-1000 ppm during the oxic period to about 3000 ppm during the anoxic period. The bottom water is close to saturation regarding calcite and undersaturation regarding aragonite during the oxygenated period, and is undersaturated regarding both calcite and aragonite during the anoxic period.

The upper 2-4 millimetres of the sediments are characterized by remarkable redox-forced changes. In the oxic conditions a small local maximum of pH is formed (**Figure 5**); this persists during the change of BBL conditions from oxic to anoxic and is more pronounced when the BBL is suboxic (**Figure 6**). According to the model, this maximum depends on the consumption of carbon dioxide during chemosynthesis and the pronouncement increases with increasing chemosynthesis by anaerobic autotrophs.

During the stagnation period, a minimum of pH forms at about 5-10 mm depth, correlated with maxima of alkalinity and DIC. An increase of alkalinity in this period is connected with sulphate reduction . The seasonal variability of alkalinity in the upper sediment (**Figure 6**) shows a concentration maximum during the anoxic period that subsequently smooths and propagates into the deeper layers, leading to lower alkalinity during the oxic period. At the boundary between the BBL and the water column the alkalinity flux changes its direction from downward in oxic conditions to upward in anoxic conditions. At the sediment-water interface boundary the alkalinity flux is directed upward with much smaller values in oxic than in anoxic conditions.

The comparison shown in **Table 2** between the main sea water alkalinity forms demonstrates that the contributions important in anoxic conditions (i.e. A_{HS}, A_{Si}, A_P, A_{NH}) remain in anoxic conditions small compared with the carbonate alkalinity. The modeled mechanism of significant alkalinity changes is connected with redox processes (listed in chapter 2.1.1) that produce or remove H^+ or OH^- and the redox processes connected with OM mineralization (i.e. sulfate reduction, Mn reduxtion and Fe reduction). Because the protolithic reactions are very fast the results of these processes reflects in the ratio between carbonate and bicarbonate in a larger degree than in production/consumption of the forms of alkalinity important in anoxic conditions.

During the oxygenated period the sediment is oversaturated with respect to calcite and precipitation of $CaCO_3$ occurs, while during the anoxic period this $CaCO_3$ dissolves (**Figure 5**). The model simulation reproduces an interesting phenomenon of an increase of the calcite saturation state in the upper 2-4 millimetres of the sediments at the beginning of the stagnation period, when oxygen starts to decrease in the BBL (**Figure 9**).

Table 2. Typical concentrations (ranges of concentrations) of alkalinity in the seawater (in μM).

		Value, μM, in oxic(/anoxic) conditions	**Source**
A_C	$[HCO_3^-] + 2[CO_3^{2-}]$	2306	Typical seawater (Millero, 1979)
A_B	$[B(OH)_4^-]$	100	Typical seawater (Dickson, 2010; Millero, 1995)
A_{OM}	DOC (15% of total)	6-75	Sea water (Canfield et al., 2005; Kepkay, 2000)
A_{HS}	$[HS^-]$	<0/50	Black Sea (Volkov and Rozanov, 2006)
A_{Si}	$[SiO(OH)_3^-]$	< 10/40	Black Sea (Volkov and Rozanov, 2006)
A_P	$[HPO_4^{2-}] + 2[PO_4^{2-}] - [H_3PO_4]$	2/7	Black Sea (Volkov and Rozanov, 2006)
A_{NH}	$[NH_3]$	<2/5	Black Sea (Volkov and Rozanov, 2006)
A_F	[HF] (total F)	68	Typical seawater (Dickson, 2010; Millero, 1995)
$[OH^-]$	$[OH^-]$	8	Typical seawater (Dickson, 2010; Millero, 1995)
$[H^+]$	$[H^+]$ (pH=8.151 NBS)	0.007	Typical seawater (Millero, 1979)
A_{HSO4}	$[HSO_4^-]$	0.0015-0.010	Typical seawater (Dickson, 2010)

Deeper in the sediment pH decreases to about 7.1, alkalinity and DIC stabilizes at 4500 μM and 4530 μM respectively, and pCO2 reaches 5500 ppm. Aragonite (in a larger degree) and Calcite (in a smaller degree) are undersaturated there. Note that according to the model assumption these sediment carbonate system distribution and variability were formed by the forcing from the upper boundary.

The model calculations clearly demonstrate an importance of redox conditions for the carbonate system (and alkalinity) changes that should therefore determine the processes of carbon transformation and transport

4.3 Bioturbation

Bioturbation plays an important role in the oxic/anoxic interface changes. We made an experiment to assess the effect of bioturbation on the distribution of the model parameters.

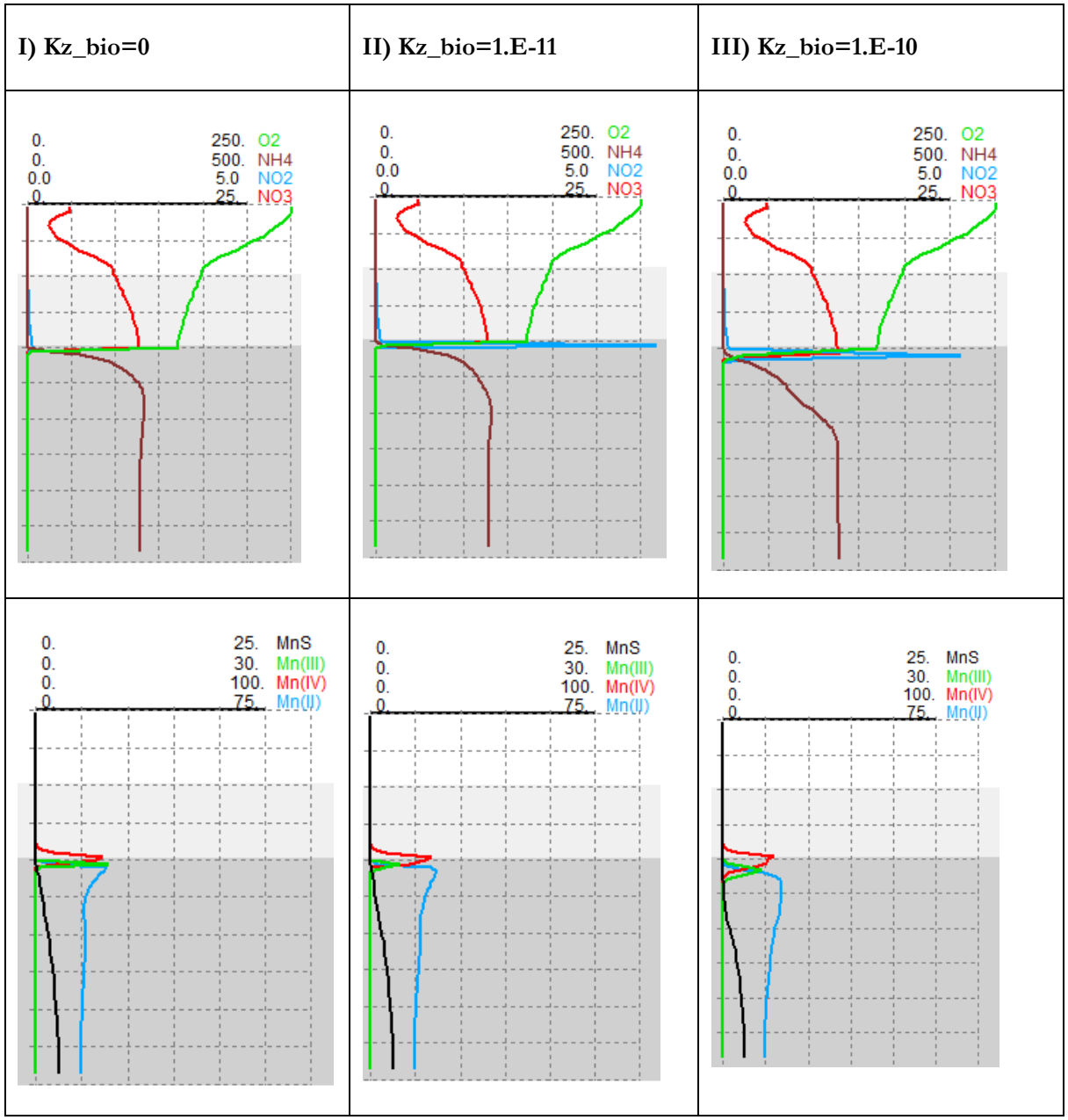

Figure 8. Modelled vertical distributions of O_2, NO_3, NO_2, NH_4, Mn(II), Mn(III), Mn(IV), MnS in day 90, winter (top row for (I) absence of bioturbation,(II) real rates of bioturbation Kz_bio=1. 10^{-11} m^2s^{-1} and (III) overpriced rate of bioturbation Kz_bio=10. 10^{-11} m^2s^{-1}). The concentrations are in µM.

Model simulation of the seasonal bottom anoxia formation was taken as a background. In the experiment 3 scenarios were simulated, here Kz_bio is coefficient of bioturbation: I) Kz_bio=0 m^2s^{-1}, II) Kz_bio=1. 10^{-11} m^2s^{-1}, III) Kz_bio=10. 10^{-11} m^2s^{-1}

Oxygen penetrates into first millimeters of sediment during events with high bioturbation (**Figure 9**), agreeably H_2S in that cases disappears there.

The model experiment showed that in case of the basic run with (II) and an absence of the bioturbation (I) the maximum depth of penetration of oxygen should is limited to 2-4 millimeters of the sediment. In case of an increased bioturbation (III) the maximum depth of penetration of oxygen increases to 8-10 mm of sediment (**Figure 8**). In case of an increased bioturnation, Mn(IV) forms in a thicker layer.

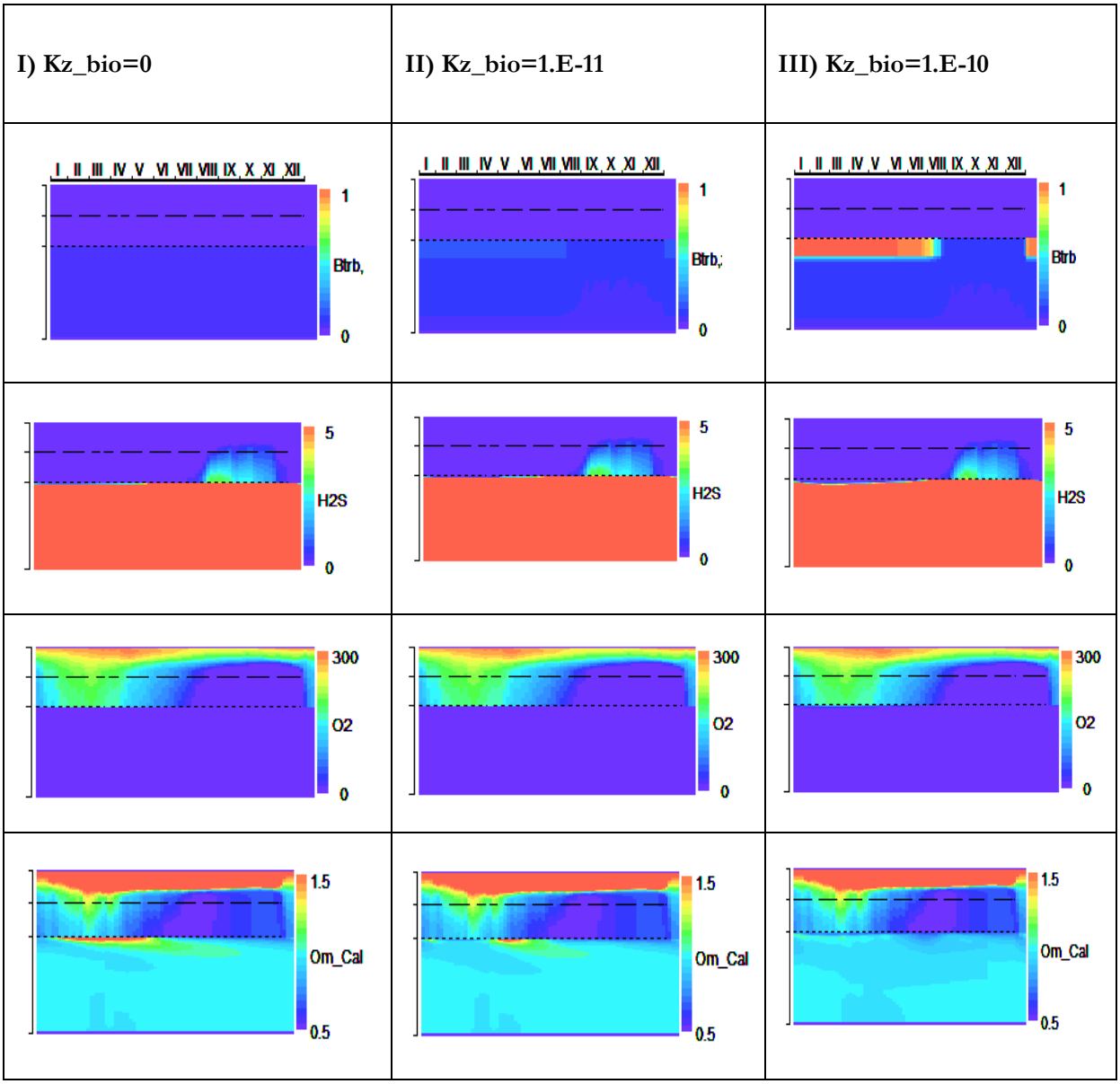

Figure 9. Modelled seasonal variability of bioturbation rates, H_2S, O_2, Calcium Saturation (top row for (I) absence of bioturbation,(II) real rates of bioturbation Kz_bio=1. 10^{-11} m^2s^{-1} and (III) overpriced rate of bioturbation Kz_bio=10. 10^{-11} m^2s^{-1}). The concentrations are in µM. The dotted line corresponds to the sediment-BBL boundary and the dashed-line to the BBL-water column boundary.

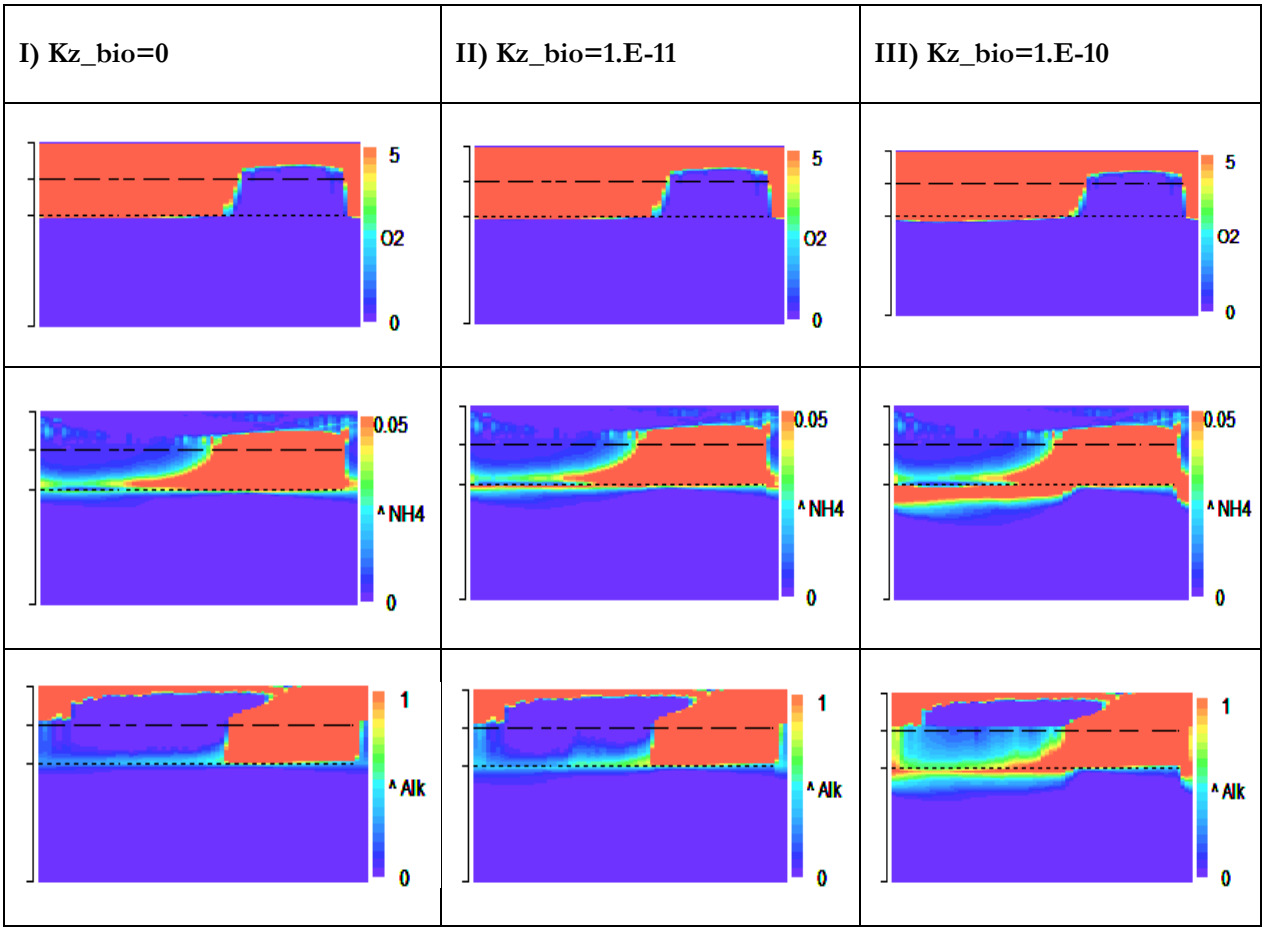

Figure 10. Modelled seasonal variability of upward fluxes of O_2, NH_4 and Alkalinity (top row for (I) absence of bioturbation,(II) real rates of bioturbation Kz_bio=1. 10^{-11} m^2s^{-1} and (III) excessive rate of bioturbation Kz_bio=10. 10^{-11} m^2s^{-1}). The concentrations are in µM.

According to the model, aragonite saturation and ammonia and alkalinity fluxes are the most sensible parameters to fluctuations of the bioturbation rates (**Figure 9**,**Figure 10**).

In absence of bioturbation (case I) there is a clear 2 -4 mm layer of calcium carbonate oversaturation, while with appearance of bioturbation this layer becomes smoother, and in anoxic period the upper 2-4-mms of the sediment are under saturated in case III.

In an absence of bioturbation (case I) the upward fluxes of ammonia in the first millimeters of the sediment is much smaller than for cases (II and III).

The flux of alkalinity also varies in three scenarios; changes mainly concern the BBL-sediment interface. With an increased bioturbation (cases II and III) the layer subjected to alkalinity flux in the sediments increases as in depth and intensity. With the basic rates of bioturbation (case II) alkalinity fluxes are detectable in the deeper 25 cm of BBL, with increased bioturbation (case III) they propagate on all BBL and on 3-4 cm of the sediment.

5. Conclusions

The extended Bottom RedOx Model, BROM, is devoted to the analysis of the complex interactions of biogeochemical processes occurring in the water column, the sediments and the BBL. In this study, we mainly focused on the processes occurring at the sediment-water interface and the BBL. Explicit description of processes in the surrounding media (i.e. the water column and the sediments) provided the boundary conditions at this main spot of interest.

The set of biogeochemical processes occurring at the sediment-water interface is complex and includes interdependences of the cycles of many chemical elements. Nevertheless, model simulations identified two key drivers: seasonality in production and destruction of OM together with seasonal mixing can explain the changes in redox conditions and the seasonal occurrence of bottom anoxia. Model results show that vertical fluxes across the BBL must be subject to significant variability, associated with distinct vertical (first of all during the stagnation period) and temporal patterns connected with the changes in redox conditions. Additionally, the simulations demonstrate that redox conditions have a significant impact on the carbonate system (and alkalinity) and on the processes of carbon transformation and transport. Bacteria play a significant role in the fate of OM due to chemosynthesis (autotrophs) and consumption of DOM (heterotrophs). This model allowed us to simulate the distributions of Mn(III), a form of Mn that has only recently been considered and has never before been included in a sedimentary biogeochemical model(Madison et al., 2013).

BROM is suitable for use in a wide variety of applications. It is capable of reproducing seasonal variations in oxygen concentration and redox state, to resolve fine scale structure of the water column, BBL and sediment, and to capture the time lags associated with rarely modelled compounds (e.g., Mn and Fe oxides role in securing of the H2S efflux, pH, alkalinity, carbonate saturation change). By virtue of its capability to predict pH values and redox state, BROM is also ideally suited to model and investigate the fate of a wider range of chemical elements and compounds. In particular, it enables accurate description of reactions that are mediated by pH and redox state, such as precipitation and dissolution of numerous compounds.

As a component of FABM the BROM can be easily coupled with different hydrodynamic models. This enables it to be used in projects on CCS reservoir leakage, methane seeps, priority substances (i.e. heavy metals, radioactive substances), sediment efflux (i.e. in mine tailing, drilling activity etc.), and coastal oxygen depletion. The source code of BROM is freely available from the repository for FABM, hosted at http://fabm.net.

6. Aknowledgements

The research leading to these results has received funding from the EC 7th Framework Programme (FP7/2007-2013) under grant agreement no 265847 ('Sub-seabed CO2 Storage: Impact on Marine Ecosystems', ECO2) and 240837 ('Research into Impacts and Safety in CO_2 Storage', RISCS), with additional development funds from FME SUCCESS, CO2Base, EEA CO2MARINE, Norwegian Research Council project no. 236658 ('New knowledge on sea deposits' NYKOS) and NIVA OA SIS project.

Table 3. Parameterization of the biogeochemical processes

Name of Process / reaction	Parameterizations
Autolysis	$AutolysisN = K_{\_PON\_DON} * PON$
Mineralization at oxic conditions (Richards, 1965) $(CH_2O)_{106}(NH_3)_{16}H_3PO_4 + 106O_2 = 106CO_2 + 16NH_3 + H_3PO_4 + 106H_2O$	$DcDM\_O2 = (1 + f_t^D(t)) * K_{ND4} * DON * F_{OX}$ $DcPM\_O2 = (1 + f_t^D(t)) * K_{NP4} * PON * Fox$ where $Fox = \frac{O2}{O2 + K\_omox\_o2}$ and $f_t^D(t) = B_{da} \frac{t^2}{t^2 + t_{da}^2}$
Manganese	
Manganese(II) oxidation (Canfield et al., 2005) $4Mn^{2+} + O_2 + 4H^+ \rightarrow 4Mn^{3+} + 2H_2O$	$Mn_{ox} = K_{Mn\_ox} * O_2 * Mn(II)$
Manganese (III) oxidation (Tebo et al., 1997) $2Mn^{3+} + 3H_2O + 0.5O_2 \rightarrow 2MnO_2 + 6H^+$	$Mn_{ox2} = K_{Mn\_ox2} * O_2 * Mn(III)$
Manganese (IV) reductions $2MnO_2 + 7H^+ + HS^- \rightarrow 2Mn^{3+} + 4H_2O + S^0$	$\mathrm{Mn_{rd}} = \mathrm{K_{Mn\_rd}} * \mathrm{Mn(IV)} * \mathrm{H_2S}$
Manganese (III) reduction $2Mn^{3+} + HS^- \rightarrow 2Mn^{2+} + S^0 + H^+$	$Mn_{rd2} = K_{Mn\_rd2} * Mn(III) * H_2S$
Solid MnS formation $Mn^{2+} + H_2S \rightarrow MnS + 2H^+$	$MnS_{form} = K_{MnS\_form} * H_2S * Mn(II)$
MnS dissolution	$MnS_{ox} = K_{MnS\_ox} * O_2 * MnS$

$MnS + 2O_2 \rightarrow Mn^{2+} + SO_4^{2-}$	
Manganese reduction for PON (Boudreau, 1996) $(CH_2O)_{106}(NH_3)_{16}H_3PO_4 + 212MnO_2 + 318CO_2 + 106H_2O \rightarrow 424HCO_3^- + 212 Mn^{2+} + 16NH_3 + H_3PO_4$	$Dc_{PM\_Mn} = K_{PON\_Mn} * PON * Mn(IV) * (1 - 0{,}5 * (\tanh(O_2 - O_{2\_S\_dn}))$
Manganese reduction for DON (Boudreau, 1996) $(CH_2O)_{106}(NH_3)_{16}H_3PO_4 + 212MnO_2 + 318CO_2 + 106H_2O \rightarrow 424HCO_3^- + 212 Mn^{2+} + 16NH_3 + H_3PO$	$Dc_{DM\_Mn} = K_{DON\_Mn} * DON * Mn(IV) * (1 - 0{,}5 * (\tanh(O_2 - O_{2\_S\_dn}))$
Iron	
Fe (II) oxidation 1(Canfield et al., 2005) $Fe^{2+} + O_2 + 4H^+ \rightarrow Fe^{3+} + 2H_2O$	$Fe_{ox} = K_{Fe_{ox}} * Fe(II) * O_2$
Fe (II) oxidation 2 (Yakushev et al., 2007) $2Fe^{2+} + MnO_2 + 2H_2O \rightarrow 2FeOOH + Mn^{2+} + 2\ H^+$	$Fe_{ox2} = K_{Fe\_ox2} * Mn(IV) * Fe(II)$
Fe (III) reduction $2Fe^{3+} + HS^- \rightarrow 2Fe^{2+} + S^0 + H^+$	$Fe_{rd} = K_{Fe\_rd} * H_2S * Fe(III)$
FeS dissolution $FeS + 2O_2 \rightarrow Fe^{2+} + SO_4^{2-}$	$FeS_{ox} = K_{FeS\_ox} * O_2 * FeS$
Formation of FeS from Fe(II) with H_2S $Fe^{2+} + H_2S + HCO_3^- \rightarrow FeS + CO_2 + H_2O + H^+$	$FeS_{form} = K_{FeS\_form} * H_2S * Fe(II)$

Iron reduction for DON (Boudreau, 1996) $(CH_2O)_{106}(NH_3)_{16}H_3PO_4$ + 424 $Fe(OH)_3$ + 742CO_2 → 848HCO_3^-+ 424 Fe^{2+}+ 318 H_2O + 16NH_3 + H_3PO_4	$DcDM_{Fe} = K_{DON\_Fe} * DON * Fe(III) * \left(1. - 0.5 * \left(1 + tanh\left(O_2 - O_{2_{s_{dn}}}\right)\right)\right)$
Iron reduction for PON (Boudreau, 1996) $(CH_2O)_{106}(NH_3)_{16}H_3PO_4$ + 424 $Fe(OH)_3$ + 742CO_2 → 848HCO_3^-+ 424 Fe^{2+}+ 318 H_2O + 16NH_3 + H_3PO_4	$DcDM_{Fe} = K_{PON\_Fe} * PON * Fe(III) * \left(1. - 0.5 * \left(1 + tanh\left(O_2 - O_{2_{s_{dn}}}\right)\right)\right)$
Nitrogen	
Nitrification (Canfield et al., 2005) 1 stage NH_4^+ + 1.5 O_2 → NO_2^- + $2H^+$ + H_2O 2 stage NO_2^- + 0.5 O_2 → NO_3^-	$Nitrif1 = K_{N42} * NH_4 * O_2 * 0.5 * (1. + tanh(O_2 - O_{2\_s\_nf}))$ $Nitrif2 = K_{N23} * NO_2 * O_2 * 0.5 * (1. + tanh\left(O_2 - O_{2_{s_{nf}}}\right))$
Anammox (Canfield et al., 2005) NO_2^- +NH_4^+→ N_2+2H_2O	$Anammox = K_{anammox} * NO_2 * NH_4 * \left(1. - 0.5 * \left(1 + tanh\left(O_2 - O_{2_{s_{dn}}}\right)\right)\right)$
OM Denitrification $(CH_2O)_{106}(NH_3)_{16}H_3PO_4$ + 84.8HNO_3 = 106CO_2 + 42.4N_2 + 148.4H_2O + 16NH_3 + H_3PO_4 (Richards, 1965)	

POM denitrification (1st stage) (Anderson et al., 1982) $1/2CH_2O + NO_3^- \rightarrow NO_2^- + 1/2H_2O + 1/2CO_2$ POM denitrification (2d stage) (Anderson et al., 1982) $3/4CH_2O + H^+ + NO_2^- \rightarrow 1/2N_2 + 5/4H_2O + 3/4CO_2$ DOM denitrification (1st stage) (Anderson et al., 1982): $1/2CH_2O + NO_3 \rightarrow NO_2^- + 1/2H_2O + 1/2CO_2$ POM denitrification (2d stage) (Anderson et al., 1982) $3/4CH_2O + H^+ + NO_2^- \rightarrow 1/2N_2 + 5/4H_2O + 3/4CO_2$	$Denitr1_{PM} = K_{N32} * PON * Fdnox \frac{NO_3}{NO_3 + K_{omno_{NO3}}}$ $Denitr2_{PM} = KN_{24} * PON * Fdonx * \frac{NO_2}{NO_2 + K_{omno\_NO2}}$ $Denitr1_{DM} = K_{N32} * DON * Fdnox * \frac{NO_3}{NO_3 + K_{omno_{NO3}}}$ $Denitr2_{PM} = KN_{24} * PON * Fdnox * \frac{NO_2}{NO_2 + K_{omno\_NO2}}$ $Fdnox = (1. - 0.5 * \left(1 + tanh\left(O_2 - O_{2_{S_{dn}}}\right)\right))$ $Denitr1 = Denitr1\_PM + Denitr1\_DM$ $Denitr2 = Denitr2\_PM + Denitr2\_DM$
Sulfur	
S^0 disproportionation (Canfield et al., 2005) $4S^0 + 3H_2O \rightarrow 2H_2S + S_2O_3^{2-} + 2H^+$	$Disprop = K_{dispro} * S^0$
HS oxidation with O_2: $2H_2S + O_2 \rightarrow 2S^0 + 2H_2O$	$HS\_ox = K_{HS\_ox} * H_2S * O_2$
S^0 oxidation with O_2: $2S^0 + O_2 + H_2O \rightarrow S_2O_3^{2-} + 2H^+$	$S^0ox = K_{S^0\_ox} * S^0 * O_2$
S^0 oxidation with NO_3: $4S^0 + 3NO_3^- + 7H_2O \rightarrow 4SO_4^{2-} + 3NH_4^+ + 2H^+$	$S^0{}_{NO3} = K_{S0\_NO3} * NO_3 * S^0$

S_2O_3 oxidation with O_2: $S_2O_3^{2-} + 2O_2 + 2OH^- \rightarrow 2SO_4^{2-} + H_2O$	$S_2O_3ox = K_{s23\_ox} * S_2O_3 * O_2$
S_2O_3 oxidation with NO_3: $S_2O_3 + NO_3^- + 2H_2O \rightarrow 2SO_4^{2-} + NH_4^+$	$S_{23\_NO3} = K_{S23\_NO_3} * NO_3 * S_2O_3$
Thiodenitrification (Schippers and Jorgensen, 2002) $3H_2S + 4NO_3^- + 6OH^+ \rightarrow 3SO_4 + 2N_2 + 6H_2O$	$sulfido = KT * H_2S * NO_3$
Sulfatereduction (Boudreau, 1996) $(CH_2O)_{106}(NH_3)_{16}H_3PO_4 + 53SO_4^{2-} = 106HCO_3^- + 16NH_3 + H_3PO_4 + 53H2S$ 1) POM sulfatereduction (1st stage): 2) DOM sulfatereduction (1st stage): 3) POM sulfatereduction (2d stage): 4) DOM sulfatereduction (2d stage):	1) $s4\_rd\_PM = K\_s4\_rd * Fsox * Fsnx * SO_4 * PON$ 2) $s4\_rd\_DM = K\_s4\_rd * Fsox * Fsnx * SO_4 * DON$ 3) $s23\_rd\_PM = K\_s23\_rd * Fsox * Fsnx * S_2O_3 * PON$ 4) $s23\_rd\_DM = K\_s23\_rd * Fsox * Fsnx * S_2O_3 * DON$ $Fsox = (1. - 0.5 * (1. + tanh(O_2 - s\_omso\_o2)))$ $Fsnx = (1. - 0.5 * (1. + tanh(NO_3 - s\_omso\_no)))$ $s4\_rd = S4\_rd\_PM + S4\_rd\_DM$ $s23\_rd = s23\_rd\_PM + s23\_rd\_DM$ $DcPM\_SO4 = {}^{16}/_{53} * (s4\_rd\_PM + s23\_rd\_PM)$! in N units $DcDM\_SO4 = {}^{16}/_{53} * (s4\_rd\_DM + s23\_rd\_DM)$
Carbon and Alkalinty	
$CaCO_3$ solubility (Luff et al., 2001)	*CaCO3_prec =k_CaCO3_prec*max(0._rk,(Om_Ar-1._rk))*
$CaCO_3$ dissolution (Luff et al., 2001)	*CaCO3_diss =CaCO3*k_CaCO3_diss*(max(0._rk,(1._rk-Om_Ar)))**4.5*

$A_T=A_C+ A_B + A_P + A_{Si} +A_{NH} +A_{HS} +A_F + [OH^-] - [H^+] + A_{OM}$	$$dAlk = \frac{(Dc_{OM_{total}} - ChemBaae - ChemBaan)}{(Knh4 + Hplus)} * Hplus + \left(\frac{(Dc_{OM_{total}} - ChemBaae - ChemBaan)}{NkP} + \frac{(fe_{rd} - fe_{ox} - fe_{ox2} + 4 * DcDM_{Fe} + 4 * DcPM_{Fe})}{2.7} - \frac{(mn_{ox2} + mn_{rd2} - mn_{ox} - mn_{rd})}{0.67}\right) * \frac{((Kp1 * Kp2 - Hplus^2) * Hplus + 2e0 * Kp1 * Kp2 * Kp3)}{\left((Hplus + Kp1) * Hplus + Kp1 * Kp2\right) * Hplus + Kp1 * Kp2 * Kp3)} + (-0.5 * mn_{rd} - 0.5 * mn_{rd2} - 0.5 * fe_{rd} - hs_{ox} - fes_{prec} + fes_{diss} - mns_{prec} + 0.5 * Disprop - sulfido + s23_{rd}) * \frac{Kh2s1}{(Kh2s1 + Hplus)} + 2.* (s4_{rd} + s23_{rd}) + \left(k_{Sipart_{diss}} * Sipart\right) * \frac{KSi}{(KSi + Hplus)} - 2 * Nitrif1 + Denitr2_{PM} + Denitr2_{DM} + mn_{ox} - 3 * mn_{ox2} + 3.* mn_{rd} - 1.* mn_{rd2} - 2.* mns_{prec} + 2.* mns_{diss} + CkN * 26.5 * (DcDM_{Mn} + DcPM_{Mn}) + fe_{ox} - fe_{ox2} - 1.* fe_{rd} - 2.* fes_{prec} + 2. * fes_{diss} + CkN * 53.* (DcDM_{Fe} + DcPM_{Fe}) - 1.* (-s0_{ox}) - 0.5 * s0_{no3} - 2 * s23_{ox} + 1.6 * sulfido - 2 * \&CaCO3\_prec + 2 * CaCO3\_diss$$
Phytoplankton	
Growth of phytoplankton	$GrowthPhy = KNF\ LimLight\ LimT\ \text{MIN}\ (LimP, LimN)\ Phy \cos((LatLight - 23.5\ sin\left(2\pi \frac{julianday - 81}{365}\right))/\ (\pi/180))$
Irradiance changing with depth	$Iz = Io * e^{(-k\_Erlov * z)}$
Influence of the Irradiance on photosynthesis	$LimLight = ({}^{Iz}/_{Iopt}) * e^{(1 - Iz/Iopt)}$
Influence of Temperature on photosynthesis	$LimT = e^{\ (bm * tem2 - cm)}$

dependence of photosynthesis on P	$LimP = \frac{(PO_4/Phy)^2}{(KPO_4 * NkP)^2 + (PO_4/Phy)^2}$
dependence of photosynthesis on NO_3	$LimNO_3 = \frac{((NO_3 + NO_2)/Phy)^2}{KNO_3{}^2 + ((NO_3 + NO_2)/Phy)^2}$
dependence of photosynthesis on NH_4	$LimNH_4 = \frac{(NH_4/Phy)^2}{KNH_4{}^2 + (NH_4/Phy)^2}$
Influence of N on photosynthesis	$LimN = LimNO_3 + Lim$
Phy excretion rate	$ExcrPhy = K_{FD} * Phy$
Phy mortality rate	$MortPhy = (KFP + 0.45 * (0.5 - 0.5 * tanh(O\_2 - 60.)) + 0.45 * (0.5 - 0.5 * tanh(O_2 - 20))) * Phy$
Zooplankton	
Grazing of *Zoo*	$Grazing = GrazPhy + GrazPOP + GrazBact$
Grazing of *Zoo* on *Phy*	$GrazPhy = KFZ * Zoo * \frac{(Phy/(Zoo + 0.0001))^2}{K_{FY}{}^2 + (Phy/(Zoo + 0.0001))^2}$
Grazing of *Zoo* on detritus	$GrazPOP = KPZ * Zoo * \frac{(Zoo + 0.0001)^2}{(PON)^2 + (Zoo + 0.0001)^2}$
Grazing of *Zoo* on bacteria	$GrazBact = GrazBaae + GrazBaanA + GrazBhae + GrazBhan$
Grazing of *Zoo* on bacteria autotrophic aerobic	$GrazBaae = KPZ * Zoo * \frac{(Baae/Zoo + 0.0001)^2}{limGrazBac^2 + (Baae/Zoo + 0.0001)^2}$
Grazing of *Zoo* on bacteria autotrophic anaerobic	$GrazBautA = KPZ * Zoo * \frac{(Baan/Zoo + 0.0001)^2}{limGrazBac^2 + (Baan/Zoo + 0.0001)^2}$

Grazing of *Zoo* on bacteria heterotrophic aerobic	$GrazBhet = KPZ * Zoo * \frac{(Bhae/Zoo + 0.0001)^2}{limGrazBac^2 + (Bhae/Zoo + 0.0001)^2}$
Grazing of *Zoo* on bacteria heterotrophic anaerobic	$GrazBhetA = 1.3 * KPZ * Zoo * \frac{(Bhan/Zoo + 0.0001)^2}{limGrazBac^2 + (Bhan/Zoo + 0.0001)^2}$
Respiration rate of Zoo	$RespZoo = KZN * Zoo$
Mortality of *Zoo*	$MortZoo = Zoo * \left(0.25 + 0.3 * \left(0.5 - 0.5 * tanh(O_2 - 20)\right) + 0.45 * \left(0.5 + 0.4 * tanh(H_2S - 10)\right)\right)$
Bacteria	
Growth rate of *Bacteria aerobic autotrophic*	$ChemBaae = 0.5 * Bae * (Nitrif1 + Nitrif2 + mn_{ox} + fe_{ox} + s23_{ox} + s0_{ox} + anammox) * \frac{(NH_4/(Baae+0.0001))^2}{limBaae^2+(NH_4/(Baae+0.0001))^2}$
Rate of mortality of *Bacteria aerobic autotrophic*	$MortBaae = Baae^2 * (0.01 + 0.899 * (0.5 * (1. - tanh(1. - H_2S))))$
Growth rate of *Bacteria aerobic heterotrophic*	$HetBhae = (DcPM_{O2} + DcDM_{O2}) * 1. * Bhae * \frac{(DON/(Bhae+0.0001))^2}{limBhae^2+(DON/(Bhae+0.0001))^2}$
Rate of mortality of *Bacteria aerobic heterotrophic*	$MortBhae = Bhae * (0.005 + 0.799 * (0.5 * (1. - tanh(1. - H_2S))))$
Growth rate of *Bacteria anaerobic autotrophic*	$ChemBaan = (mn\_rd + mn\_rd2 + fe\_rd + hs\_ox + sulfido) * 0.1 * Baa * \frac{(NH4/(Baa + 0.0001))^2}{limBaan^2 + (NH4/(Baan + 0.0001))^2}$
Rate of mortality of *Bacteria anaerobic autotrophic*	$MortBaan = 0.01 * \text{Baan}$
Growth rate of *Bacteria anaerobic heterotrophic*	$HetBhan = (DcPM\_NOX + DcDM\_NOX + DcPM\_SO_4 + DcDM\_SO_4) * 0.8 * Bhan * \frac{(DON/(Bhan + 0.0001))^2}{limBhan^2 + (DON/(Bhan + 0.0001))^2}$
Rate of mortality of *Bacteria anaerobic heterotrophic*	$MortBhan = Bhan * (0.01 + 0.899 * (0.5 + 0.5 * (tanh(1. - O_2))))$

Table 4. Parameters names, notations, values and units of the coefficients used in the model

Parameter	Notation	Units	Value
Mn and Fe			
Mn(II) oxidation with O_2 constant	$K_{\_mn\_ox}$	d^{-1}	0.3
Mn(IV) reduction with Sulfide constant	$K_{\_mn\_rd}$	d^{-1}	0.4
Mn(III) oxidation with O_2 constant	$K_{\_mn\_ox2}$	d^{-1}	0.2
Mn(III) reduction with sulfide constant	$K_{\_mn\_rd2}$	d^{-1}	0.2
formation of MnS from Mn2 with sulfide constant	$K_{\_mns\_prec}$	d^{-1}	$2*10^{-5}$
dissolution of MnS to Mn2 and H_2S	$K_{\_mns\_diss}$	d^{-1}	10^{-4}
MnS oxidation with O_2 constant	$K_{\_mns\_ox}$	d^{-1}	2
DON Oxidation with Mn(IV)	$K_{\_DON\_Mn}$	d^{-1}	10^{-4}
PON Oxidation with Mn(IV) constant	$K_{\_PON\_Mn}$	d^{-1}	10^{-4}
Fe oxidation with O_2 constant	$K_{\_fe\_ox}$	d^{-1}	0.5
Fe oxidation with MnO_2 constant	$K_{\_fe\_ox2}$	d^{-1}	0.1
Fe(III) reduction with Sulfide constant	$K_{\_fe\_rd}$	d^{-1}	0.2
Formation of FeS to Fe2 and H_2S	$K_{\_FeS\_diss}$	d^{-1}	$3*10^{-5}$
Precipitation of FeS from Fe(II) with H_2S	$K_{\_FeS\_prec}$	d^{-1}	$4*10^{-4}$
DON oxidation with Fe(III) constant	$K_{\_DON\_Fe}$	d^{-1}	$5*10^{-5}$
PON oxidation with Fe(III) constant	$K_{\_PON\_Fe}$	d^{-1}	10^{-5}
Sulphur			
H_2S oxidation of with O_2	$K_{\_hs\_ox}$	d^{-1}	0.5
S^0 oxidation of with O_2	$K_{\_s0\_ox}$	d^{-1}	0.02
S^0 oxidation of with NO_3	$K_{\_S0\_NO3}$	d^{-1}	0.2
S_2O_3 oxidation with O_2	$K_{\_s23\_ox}$	d^{-1}	0.01
S_2O_3 oxidation with NO_3	$K_{\_s23\_NO3}$	d^{-1}	0.01
Sulfate reduction			
sulfate reduction with sulfate	$K_{\_s4\_rd}$	d^{-1}	$1*10^{-5}$
sulfate reduction with thiosulfate	$K_{\_s23\_rd}$	d^{-1}	$5*10^{-3}$
S^0 disproportionation			
Specific rate of S^0 disproportionation	K_{dispro}	d^{-1}	10^{-3}
Nitrogen			
DON oxidation of with O_2	$K_{\_DON\_ox}$	d^{-1}	0.01
PON oxidation of with O_2	$K_{\_PON\_ox}$	d^{-1}	0.002
Temperature control coefficient for OM decay	Tda		13
Temperature control coefficient for OM decay	beta_da		20
Half-saturation constant of O_2 for OM mineralization	$K_{\_omox\_o2}$	uM	1
Decomposition of *PON* to *DON*	$K_{\_PON\_DON}$	d^{-1}	0.1
Strength of ammonium inhibition of nitrate uptake constant	K_{psi}		1.46
Half saturation constant for uptake of NO_3+NO_2	K_{NO3}	µM	0.25

Half saturation constant for uptake of NH_4	K_{NH4}	µM	0.02
Specific rate of decomposition of *DON*	K_{ND4}	d^{-1}	0.005
Specific rate of decomposition of *PON*	K_{NP4}	d^{-1}	0.05
Nitrification			
Specific rate of the 1st stage of nitrification	K_{N42}	d^{-1}	0.1
Specific rate of the 2d stage of nitrification	K_{N23}	d^{-1}	0.1
Denitrification			
Specific rate of 1st stage of denitrification	K_{N32}	d^{-1}	0.20
Specific rate of 2d stage of denitrification	K_{N24}	d^{-1}	0.25
Half-saturation of NO_2 for denitrification	$k_{\_omno\_no3}$	µM N	0
Half-saturation of NO_2 for denitrification	$k_{\_omno\_no2}$	µM N	0
Thiodenitrification			
Thiodenitrification constant	K_T	$\mu M^{-1}d^{-1}$	0.9
Anammox			
Anammox constant	$K_{annamox}$	d^{-1}	0.8
Phosphorus			
Half-saturation constant for uptake of PO_4	K_{PO4}	µM	0.02
Oxygen			
Half-saturation for nitrification	O2s_nf		4.488
Half-saturation for denitrification	O2s_dn		10
threshold of O_2 for OM mineralization	s_omox_o2		0.01
threshold of O_2 for OM denitrification	s_omno_o2		25
threshold of O_2 for OM sulfate reduction	s_omso_o2		25
threshold of NOx for OM sulfate reduction	s_omso_no		5
Calcium			
CaCO3 dissolution rate	$K_{\_CaCO3\_diss}$	d^{-1}	3
CaCO3 precipitation rate	$k_{\_CaCO3\_prec}$	d^{-1}	10^{-4}
Phytoplankton			
Maximum specific growth rate	K_{NF}	d^{-1}	2
Extinction coefficientt	K_Erlov	m^{-1}	0.05
Incident light	I_0	W m^{-2}	80
Optimal light	I_{opt}	W m^{-2}	25
Coefficient for growth dependence on t	*bm*		0.12
Coefficient for growth dependence on t	cm		1.4
Attenuation constant for the self-shading effect	Kc	m^2/mmol N	0.03
Specific respiration rate	K_{FN}	d^{-1}	0.04
Specific rate of mortality	K_{FP}	d^{-1}	0.10
Specific rate of excretion	K_{FD}	d^{-1}	0.01
Zooplankton			
Maximum specific rate of grazing of *Zoo* on *Phy*	K_{FZ}	d^{-1}	1.0
Half-saturation constant for the grazing of *Zoo* on *Phy* for	K_{FY}		1.1

Phy/*Zoo* ratio			
Maximum specific rate of grazing of *Zoo* on *POP*	K_{PZ}	d^{-1}	0.7
Specific respiration rate	K_{ZN}	d^{-1}	0.02
Half-saturation constant for the grazing of *Zoo* on *POP* in dependence to ratio *POP*/*Zoo*	K_{PP}		0.2
Maximum specific rate of mortality of *Zoo*	K_{ZP}	d^{-1}	0.02
Food absorbency for zooplankton	U_z		0.5
Ratio between dissolved and particulate excretes of zooplankton	H_z		0.5
Limiting parameter for bacteria grazing by Zoo	limGrazBac		2
Limiting parameter for bacteria anaerobic heterotrophic	limBhan		2
Limiting parameter for bacteria aerobic heterotrophic	limBhae		5
Limiting parameter for bacteria anaerobic autotrophic	limBaan		2
Limiting parameter for bacteria aerobic autotrophic	limBaae		2
Sinking			
Rate of sinking of Phy	W_{Phy}	m d^{-1}	0.1
Rate of sinking of Zoo	W_{Zoo}	m d^{-1}	1.0
Rate of sinking of detritus	W_{sed}	m d^{-1}	5
Rate of sinking of bacteria (*Bhe,Bae,Bha,Baa*)	W_{Bact}	m d^{-1}	0.4
Rate of accelerated sinking of particles with settled Mn hydroxides	W_M	m d^{-1}	7

Table 5. Rates of biogeochemical production/consumption of the model compartments

Oxygen (O_2)	R_{O2} = *(GrowthPhy -DcDM_O2 -DcPM_O2 -RespZoo) OkN -0.5 mn_ox - 0.25 mn_ox2 -0.25 fe_ox -2. mns_ox -2. fes_ox -0.5 hs_ox -0.5 s0_ox -s23_ox -1.5 Nitrif1 -0.5 Nitrif2 -(DcDM_O2 -DcPM_O2 +GrowthPhy -RespZoo) OkN*
Phosphate (PO_4)	R_{PO4}=*(DcDM_O2+DcPM_O2+DcPM_NOX+DcDM_NOX +DcDM_SO4+DcPM_SO4+ DcDM_Mn +DcPM_Mn +DcDM_Fe +DcPM_Fe -Chemos-ChemosA-GrowthPhy+RespZoo)/NkP -(fe_ox +fe_ox2)/2.7-(mn_ox +mn_rd)/0.67 +fe_rd /2.7+(mn_ox2 + mn_rd2) /0.67*
Particulate Organic Nitrogen (PON)	R_{PON}= *-autolis -DcPM_O2 -DcPM_NOX -DcPM_SO4 -DcPM_Mn -DcPM_Fe +MortBaut +MortBautA +MortBhet +MortBhetA +MortPhy +MortZoo +Grazing *(1.-Uz)*(1.-Hz)-GrazPOP*
Dissolved Organic Phosphorus (DON)	R_{DON}= *autolis -DcDM_O2 -DcDM_NOX -DcDM_ -DcDM_Mn -DcDM_Fe -Hetero -HeteroA+ExcrPhy +Grazing *(1.-Uz)*Hz*
Ammonia (NH_4)	R_{NH4}= *DcDM_O2 +DcPM_O2 +DcPM_NOX +DcDM_NOX + DcDM_Mn +DcPM_Mn +DcDM_Fe +DcPM_Fe +DcDM_SO4 +DcPM_SO4 -Nitrif1 -anammox +RespZoo -GrowthPhy *(LimNH4 /LimN)-Chemos -ChemosA*
Nitrite (NO_2)	R_{NO2}= *Nitrif1 -Nitrif2 +Denitr1 -Denitr2 -anammox -GrowthPhy *(LimNO3 /LimN) (NO2 /(NO2 + NO3))*
Nitrate (NO_3)	R_{NO3}= *Nitrif2 -Denitr1 -sulfido *1.25 -GrowthPhy *(LimNO3 /LimN) (NO3 /(NO2 + NO3))*
Hydrogen sulphide (H_2S)	R_{H2S} = *-0.5 mn_rd -0.5 mn_rd2 -0.5 fe_rd -hs_ox -fes_form -mns_form +0.5 Disprop -sulfido +s23_rd*
Elemental sulphur (S^0)	*RS0 = hs_ox +0.5 mn_rd +0.5 mn_rd2+0.5 fe_rd -s0_ox -Disprop-*S_{0_NO3}
Thiosulfate (S_2O_3)	R_{S2O3} = *0.5 s0_ox -0.5 s23_ox +0.25 Disprop +0.5 s4_rd -0.5 s23_rd -*S_{23_NO3}
Sulfate (SO_4)	R_{SO4} = *sulfido -s4_rd +s23_ox +fes_ox +mns_ox*
Bivalent manganese (Mn(II))	R_{Mn2} = *- mn_ox +mn_rd2 -mns_form +mns_ox +fe_ox2 +2. DcDM_Mn +2. DcPM_Mn*
Quadrivalent manganese (Mn(IV))	R_{Mn4} = *mn_ox2 -mn_rd -fe_ox2 -2. DcDM_Mn -2. DcPM_Mn*
Trivalent manganese (Mn(III))	R_{Mn3} = *mn_ox - mn_ox2 + mn_rd – mn_rd2*
Manganese sulfide (MnS)	R_{MnS} = *mns_form - mns_ox*
Bivalent iron (Fe(II))	R_{Fe2} = *- fe_ox -fe_ox2 +fe_rd -fes_form +fes_ox +4. DcDM_Fe +4. DcPM_Fe*

Trivalent iron (Fe(III))	$R_{Fe3} = fe\_ox + fe\_ox2 - fe\_rd - 4.\ DcDM\_Fe - 4.\ DcPM\_Fe$
Iron sulfide (FeS)	$R_{FeS} = fes\_form - fes\_ox$
Dissolved Inorganic Carbon (DIC)	$R_{DIC} = (DcDM\_O2 + DcPM\_O2 + DcPM\_NOX + DcDM\_NOX + DcDM\_SO4 + DcPM\_SO4 + DcDM\_Mn + DcPM\_Mn + DcDM\_Fe + DcPM\_Fe - Chemos - ChemosA - GrowthPhy + RespZoo)\ CkN$
Phytoplankton (Phy)	$R_{Phy} = GrowthPhy(1 - K_{FN}) - MortPhy - ExcrPhy - GrasPhy$
Zooplankton (Zoo)	$R_{Zoo} = Grazing * U_z - MortZoo - K_{ZN} * Zoo$
Aerobic heterotrophic bacteria (Bhe)	$R_{Bhe} = C_{Bhe} - Mort_{Bhe} - Graz_{Bhe}$
Aerobic autotrophic bacteria (Bae)	$R_{Bae} = C_{Bae} - Mort_{Bae} - Graz_{Bae}$
Anaerobic heterotrophic bacteria (Bha)	$R_{Bha} = C_{Bha} - Mort_{Bha} - Graz_{Bha}$
Anaerobic autotrophic bacteria (Baa)	, $R_{Baa} = C_{Baa} - Mort_{Baa} - Graz_{Baa}$

where NkP=16 is the N:P ratio, OkP=106 is the O:P ratio, CkN=8 is the C:N ratio, .

7. References

Anderson, J.J., Okubo, A., Robbins, A.S. and Richards, F.A., 1982. A model for nitrite and nitrate distributions in oceanic oxygen minumum zones. Deep-Sea Research 29(9): 1113-1140.

Blackwelder, P., Hood, T., AlvarezZarikian, C., Nelsen, T.A. and McKee, B., 1996. Benthic foraminifera from the NECOP study area impacted by the Mississippi River plume and seasonal hypoxia. Quaternary International, 31: 19-36.

Bolding, K., Burchard, H., Pohlmann, T. and Stips, A., 2002. Turbulent mixing in the Northern North Sea: a numerical model study. Continental Shelf Research, 22(18-19): 2707-2724.

Boudreau, B.P., 1996. A method-of-lines code for carbon and nutrient diagenesis in aquatic sediments. Computers & Geosciences, 22(5): 479-496.

Bruggeman, J. and Bolding, K., 2014. A general framework for aquatic biogeochemical models. Environmental Modelling & Software, 61: 249-265.

Canfield, D.E. et al., 1993. Pathways of organic carbon oxidation in 3 continental margins. Marine Geology, 113(1-2): 27-40.

Canfield, D.E., Thamdrup, B. and Kristensen, E., 2005. Aquatic geomicrobiology. Adv. Mar. Biol, 48: 1-600.

Cooper, D.C. and Morse, J.W., 1996. The chemistry of Offatts Bayou, Texas: A seasonally highly sulfidic basin. Estuaries, 19(3): 595-611.

Couture, R.-M., Shafei, B., Van Cappellen, P., Tessier, A. and Gobeil, C., 2010. Non-Steady State Modeling of Arsenic Diagenesis in Lake Sediments. Environmental Science & Technology, 44(1): 197-203.

Debolskaya, E.I., Yakushev, E.V. and Kuznetsov, I.S., 2008. Analysis of the hydrophysical structure of the Sea of Azov in the period of the bottom anoxia development. Journal of Marine Systems, 70(3-4): 300-307.

Diaz, R.J. and Rosenberg, R., 2008. Spreading dead zones and consequences for marine ecosystems. Science, 321(5891): 926-929.

Dickson, A.G., 1992. The development of the alkalinity concept in marine chemistry. Marine chemistry, 40(1): 49-63.

Dickson, A.G., 2010. The carbon dioxide system in seawater: equilibrium chemistry and measurements. Guide to best practices for ocean acidification research and data reporting, 1: 17-40.

He, Y., Stonev, E.V., Yakushev, E. and Staneva, J., 2012. Black Sea biogeochemistry: Response to decadal atmospheric variability during 1960-2000 inferred from numerical modeling. Marine Environmental Research, 77: 90-102.

Jorgensen, B.B., Bang, M. and Blackburn, T.H., 1990. Anaerobic mineralization in marine sediments from the Baltic Sea - North Sea transition. Marine Ecology Progress Series, 59(1-2): 39-54.

Jourabchi, P., Meile, C., Pasion, L.R. and Van Cappellen, P., 2008. Quantitative interpretation of pore water O2 and pH distributions in deep-sea sediments. Geochimica et Cosmochimica Acta, 72(5): 1350-1364.

Kamyshny, A., Jost, G., Yakushev, E. and Podymov, O., 2013. Role of Sulfide Oxidation Intermediates in the Redox Balance of the Oxic–Anoxic Interface of the Gotland Deep, Baltic Sea. In: E.V. Yakushev (Editor), Chemical Structure of Pelagic Redox Interfaces. The Handbook of Environmental Chemistry. Springer Berlin Heidelberg, pp. 95–120.

Katsev, S., Chaillou, G., Sundby, B. and Mucci, A., 2007. Effects of progressive oxygen depletion on sediment diagenesis and fluxes: A model for the lower St. Lawrence River Estuary. Limnology and Oceanography, 52(6): 2555-2568.

Kepkay, P.E., 2000. Colloids and the ocean carbon cycle, Marine Chemistry. Springer, pp. 35-56.

Konovalov, S.K., Murray, J.W., Luther, G.W. and Tebo, B.M., 2006. Processes controlling the redox budget for the oxic/anoxic water column of the Black Sea. Deep-Sea Research Part Ii-Topical Studies in Oceanography, 53(17-19): 1817-1841.

Lewis, E., Wallace, D. and Allison, L.J., 1998. Program developed for CO2 system calculations. Carbon Dioxide Information Analysis Center, managed by Lockheed Martin Energy Research Corporation for the US Department of Energy.

Linke, P., Haeckel, M., Schneider v. Deimling, J. et al.,, 2014. Fluxes of CO2 from natural seep sites and Sleipner storage site.

Luff, R., Haeckel, M. and Wallmann, K., 2001. Robust and fast FORTRAN and MATLAB® libraries to calculate pH distributions in marine systems. Computers & Geosciences, 27(2): 157-169.

Madison, A.S., Tebo, B.M., Mucci, A., Sundby, B. and Luther, G.W., III, 2013. Abundant Porewater Mn(III) Is a Major Component of the Sedimentary Redox System. Science, 341(6148): 875-878.

McCarthy, M.J., McNeal, K.S., Morse, J.W. and Gardner, W.S., 2008. Bottom-water hypoxia effects on sediment-water interface nitrogen transformations in a seasonally hypoxic, shallow bay (Corpus christi bay, TX, USA). Estuaries and Coasts, 31(3): 521-531.

Millero, F.J., 1979. The thermodynamics of the carbonate system in seawater. Geochimica Et Cosmochimica Acta, 43(10): 1651-1661.

Millero, F.J., 1995. Thermodynamics of the carbon dioxide system in the oceans. Geochimica et Cosmochimica Acta, 59(4): 661-677.

Morse, J.W. and Eldridge, P.M., 2007. A non-steady state diagenetic model for changes in sediment biogeochemistry in response to seasonally hypoxic/anoxic conditions in the "dead zone" of the Louisiana shelf. Marine Chemistry, 106(1-2): 239-255.

Pavlidou, A. et al., 2013. Biogeochemical Characteristics in the Elefsis Bay (Aegean Sea, Eastern Mediterranean) in Relation to Anoxia and Climate Changes. In: E.V. Yakushev (Editor), Chemical Structure of Pelagic Redox Interfaces. The Handbook of Environmental Chemistry. Springer Berlin Heidelberg, pp. 161-201.

Pena, M., Katsev, S., Oguz, T. and Gilbert, D., 2010. Modeling dissolved oxygen dynamics and hypoxia. Biogeosciences, 7(3): 933-957.

Queirós, A.M., Norling K., Amaro T. et al.,, 2014. Potential impact of CCS leakage on marine communities.

Rabalais, N.N., Turner, R.E. and Scavia, D., 2002. Beyond science into policy: Gulf of Mexico hypoxia and the Mississippi River. Bioscience, 52(2): 129-142.

Richards, F., 1965. Anoxic basins and fjords. In: J.P.a.S. Riley, G. (Editor), Chemical Oceanography. Academic Press, NY, pp. 611-645.

Richardson, K. and Jørgensen, B.B., 1996. Eutrophication: Definition, History and Effects, Eutrophication in Coastal Marine Ecosystems. American Geophysical Union, pp. 1-19.

Roden, E.E. and Tuttle, J.H., 1992. Sulfide release from estuarine sediments underlying anoxic bottom water. Limnology and Oceanography, 37(4): 725-738.

Roy, R.N. et al., 1993. The dissociation constants of carbonic acid in seawater at salinities 5 to 45 and temperatures 0 to 45°C. . Marine Chemistry, 44(2-4): 249-267.

Schippers, A. and Jorgensen, B.B., 2002. Biogeochemistry of pyrite and iron sulfide oxidation in marine sediments. Geochimica Et Cosmochimica Acta, 66(1): 85-92.

Sell, K.S. and Morse, J.W., 2006. Dissolved Fe2+ and Sigma H2S behavior in sediments seasonally overlain by hypoxic-to-anoxic waters as determined by CSV microelectrodes. Aquatic Geochemistry, 12(2): 179-198.

SenGupta, B.K., Turner, R.E. and Rabalais, N.N., 1996. Seasonal oxygen depletion in continental-shell waters of Louisiana: Historical record of benthic foraminifers. Geology, 24(3): 227-230.

Soetaert, K., Herman, P.M.J. and Middelburg, J.J., 1996. A model of early diagenetic processes from the shelf to abyssal depths. Geochimica Et Cosmochimica Acta, 60(6): 1019-1040.

Stanev, E., He, Y., Staneva, J. and Yakushev, E., 2014. The Black Sea biogeochemistry: focus on temporal and spatial variability of oxygen. Biogeosciences Discussions, 11(1): 281-336.

Sternbeck, J., 1995. Manganese cycling in a eutrophic lake—rates and pathways. Aquatic Geochemistry, 1(4): 399-426.

Tebo, B.M., Ghiorse, W.C., van Waasbergen, L.G., Siering, P.L. and Caspi, R., 1997. Bacterially mediated mineral formation; insights into manganese (II) oxidation from molecular genetic and biochemical studies. Reviews in Mineralogy and Geochemistry, 35(1): 225-266.

Van Cappellen, P. and Wang, Y.F., 1996. Cycling of iron and manganese in surface sediments: A general theory for the coupled transport and reaction of carbon, oxygen, nitrogen, sulfur, iron, and manganese. American Journal of Science, 296(3): 197-243.

Van Der Loeff, M.M.R. and Boudreau, B.P., 1997. The effect of resuspension on chemical exchanges at the sediment-water interface in the deep sea - A modelling and natural radiotracer approach. Journal of Marine Systems, 11(3-4): 305-342.

Volkov, I. and Rozanov, A., 2006. Fundamentals of biohydrochemistry of anoxic basins. Oceanology, 46(6): 803-816.

Wanninkhof, R., 2014. Relationship between wind speed and gas exchange over the ocean revisited. Limnology and Oceanography-Methods, 12: 351-362.

Wolf-Gladrow, D.A., Zeebe, R.E., Klaas, C., Körtzinger, A. and Dickson, A.G., 2007. Total alkalinity: The explicit conservative expression and its application to biogeochemical processes. Marine Chemistry, 106(1): 287-300.

Yakushev, E. and Debolskaya, E., 1998. Particulate manganese as a main factor of oxidation of hydrogen sulfide in redox zone of the Black Sea, Proc. Konstantin Fedorov Memorial Symposium. Oceanic Fronts and Related Phenomena, pp. 18-22.

Yakushev, E., Pakhomova, S., Sorenson, K. and Skei, J., 2009. Importance of the different manganese species in the formation of water column redox zones: Observations and modeling. Marine Chemistry, 117(1-4): 59-70.

Yakushev, E.V., 2006. Redox Layer Model (ROLM): A Tool for Analysis of the Water Column Oxic/anoxic Interface Processes. Institut für Meereskunde Warnemhunde.

Yakushev, E.V. et al., 2011. Modeling the influence of oxygenated inflows on the biogeochemical structure of the Gotland Sea, central Baltic Sea: Changes in the distribution of manganese. Computers & Geosciences, 37(4): 398-409.

Yakushev, E.V. and Newton, A., 2013. Introduction: Redox Interfaces in Marine Waters. In: E.V. Yakushev (Editor), Chemical Structure of Pelagic Redox Interfaces. The Handbook of Environmental Chemistry. Springer Berlin Heidelberg, pp. 1-12.

Yakushev, E.V. et al., 2007. Analysis of the water column oxic/anoxic interface in the Black and Baltic seas with a numerical model. Marine Chemistry, 107(3): 388-410.

Zeebe, R.E. and Wolf-Gladrow, D., 2001. CO2 in Seawater: Equilibrium, Kinetics, Isotopes: Equilibrium, Kinetics, Isotopes. Elsevier.

NIVA: Norway's leading centre of competence in aquatic environments

NIVA provides government, business and the public with a basis for preferred water management through its contracted research, reports and development work. A characteristic of NIVA is its broad scope of professional disciplines and extensive contact network in Norway and abroad. Our solid professionalism, interdisciplinary working methods and holistic approach are key elements that make us an excellent advisor for government and society.

NIVA
Norwegian Institute for Water Research

Gaustadalléen 21 • NO-0349 Oslo, Norway
Telephone: +47 22 18 51 00 • Fax: 22 18 52 00
www.niva.no • post@niva.no